UNIVERSITY OF AMSTERDAM

UvA-DARE (Digital Academic Repository)

Probing light sterile neutrinos in left-right symmetric models with displaced vertices and neutrinoless double beta decay

de Vries, Jordy; Dreiner, Herbi K.; Groot, Jelle; Günther, Julian Y.; Wang, Zeren Simon

DOI
10.48550/arXiv.2406.15091
10.1007/JHEP04(2025)007

Publication date
2025

Document Version
Final published version

Published in
Journal of High Energy Physics

License
CC BY

Link to publication

Citation for published version (APA):
de Vries, J., Dreiner, H. K., Groot, J., Günther, J. Y., & Wang, Z. S. (2025). Probing light sterile neutrinos in left-right symmetric models with displaced vertices and neutrinoless double beta decay. *Journal of High Energy Physics*, *2025*(4), Article 7. https://doi.org/10.48550/arXiv.2406.15091, https://doi.org/10.1007/JHEP04(2025)007

General rights
It is not permitted to download or to forward/distribute the text or part of it without the consent of the author(s) and/or copyright holder(s), other than for strictly personal, individual use, unless the work is under an open content license (like Creative Commons).

Disclaimer/Complaints regulations
If you believe that digital publication of certain material infringes any of your rights or (privacy) interests, please let the Library know, stating your reasons. In case of a legitimate complaint, the Library will make the material inaccessible and/or remove it from the website. Please Ask the Library: https://uba.uva.nl/en/contact, or a letter to: Library of the University of Amsterdam, Secretariat, P.O. Box 19185, 1000 GD Amsterdam, The Netherlands. You will be contacted as soon as possible.
UvA-DARE is a service provided by the library of the University of Amsterdam (https://dare.uva.nl)

Download date:18 Nov 2026

Published for SISSA by Springer

Received: July 12, 2024
Revised: January 9, 2025
Accepted: March 3, 2025
Published: April 1, 2025

Probing light sterile neutrinos in left-right symmetric models with displaced vertices and neutrinoless double beta decay

Jordy de Vries,[a,b] **Herbi K. Dreiner**,[c] **Jelle Groot**,[a,b] **Julian Y. Günther**[c] **and Zeren Simon Wang**[d]

[a] *Institute for Theoretical Physics Amsterdam and Delta Institute for Theoretical Physics, University of Amsterdam, Science Park 904, 1098 XH Amsterdam, The Netherlands*
[b] *Nikhef, Theory Group, Science Park 105, 1098 XG, Amsterdam, The Netherlands*
[c] *Bethe Center for Theoretical Physics & Physikalisches Institut der Universität Bonn, Nußallee 12, 53115 Bonn, Germany*
[d] *School of Physics, Hefei University of Technology, Hefei 230601, China*

E-mail: j.devries4@uva.nl, dreiner@uni-bonn.de, j.groot4@uva.nl, guenther@physik.uni-bonn.de, wzs@hfut.edu.cn

Abstract: An investigation of relatively light (GeV-scale), long-lived right-handed neutrinos is performed within minimal left-right symmetric models using the neutrino-extended Standard Model Effective Field Theory framework. Light sterile neutrinos can be produced through rare decays of kaons, D-mesons, and B-mesons at the Large Hadron Collider (LHC) and the Long-Baseline Neutrino Facility (LBNF) of Fermilab. Their decays could result in displaced vertices, which can be reconstructed. By performing Monte-Carlo simulations, we assess the sensitivities of the future LHC far-detector experiments ANUBIS, CODEX-b, FACET, FASER(2), MoEDAL-MAPP1(2), MATHUSLA, the recently approved beam-dump experiment SHiP, and the upcoming neutrino experiment DUNE at the LBNF, to the right-handed gauge-boson mass M_{W_R} as functions of neutrino masses. We find that DUNE and SHiP could be sensitive to right-handed gauge-boson masses up to $\sim 25\,\text{TeV}$. We compare this reach to indirect searches such as neutrinoless double beta decay, finding that displaced-vertex searches are very competitive.

Keywords: Left-Right Models, New Light Particles, Sterile or Heavy Neutrinos, Baryon/Lepton Number Violation

ArXiv ePrint: 2406.15091

Open Access, © The Authors.
Article funded by SCOAP^3.

https://doi.org/10.1007/JHEP04(2025)007

Contents

1 Introduction **1**

2 Minimal left-right symmetric model **4**
2.1 Seesaw phenomenology 7

3 Standard model effective field theory extended by sterile neutrinos **10**
3.1 The effective neutrino Lagrangian 10

4 Sterile-neutrino production **12**
4.1 Minimal mixing scenario 12
4.2 Left-right symmetric models 13

5 Sterile-neutrino decay **15**
5.1 Left-right symmetric models 16

6 Neutrinoless double beta decay **19**

7 Collider and fixed-target analysis **22**

8 Numerical results **24**
8.1 Type-II seesaw benchmark scenarios 24
8.2 Type-I seesaw benchmark scenarios 26

9 Conclusions **28**

1 Introduction

One of the big puzzles of the Standard Model (SM) is the mechanism behind the generation of neutrino masses. Astrophysical [1, 2] and laboratory [3–6] neutrino flavor-oscillation experiments have unequivocally shown that SM neutrino masses are non-vanishing. The SM electroweak symmetry group $\mathrm{SU}(2)_L \otimes \mathrm{U}(1)_Y$ cannot accommodate non-zero left-handed (LH) neutrino mass terms at the renormalizable level. However, adding right-handed (RH) neutrino fields, which do not transform under SM gauge symmetries, allows for non-zero renormalizable neutrino mass terms. Through a Yukawa term that couples a RH neutrino field to a SM Higgs field and a LH (SM) neutrino field, electroweak symmetry breaking (EWSB) can generate Dirac masses for the neutrinos in an analogous manner to the other (massive) SM fermions. However, a Majorana mass term is allowed for the RH neutrinos in this case.

The combination of both Dirac and Majorana mass terms leads to Majorana neutrino mass eigenstates and a split spectrum; this is usually referred to as the seesaw mechanism [7–17]. In addition to the three light active neutrinos, there must exist at least two (three if the lightest active neutrino is not massless) heavier Majorana neutrinos [18–20]. If these additional neutrinos have masses above the eV scale, their interactions are suppressed and

JHEP04(2025)007

are often denoted as sterile neutrinos or heavy neutral leptons (HNLs) [21–23] (for a review see ref. [24]). Within this minimal scenario, the mass scale of sterile neutrinos is not well constrained. It can range from very heavy (10^{15} GeV) to very light (eV), and the sterile-neutrino pairs can either be almost mass-degenerate or have a large mass hierarchy. A generic prediction, however, is that active neutrinos are Majorana and that processes violating lepton number (L) by two units are possible.

Recently, there has been much interest in sterile neutrinos with GeV-scale masses (see, for instance, refs. [25–30]), especially in the context of searches for long-lived particles (LLPs) (see refs. [31–34] for recent reviews of LLPs). In the minimal scenario where the only interactions between the sterile neutrinos and the SM particles are mediated by the active-sterile neutrino mixings U^2, the current bounds on the sterile neutrinos in this mass range hint that these sterile neutrinos, if existent, would be long-lived [24, 35, 36]. Beam-dump, neutrino, and collider experiments produce mesons in very large numbers. These mesons can produce sterile neutrinos with masses in the MeV-GeV range through rare decays. With a long lifetime, these sterile neutrinos travel a macroscopic distance before potentially decaying inside a detector volume placed a few to a few hundred meters away. Past studies have investigated these minimal scenarios extensively and indicated that (proposed) future experiments such as `CODEX-b` [37, 38], `DarkQuest` [39], `DUNE` [40–46], `ANUBIS` [47, 48], `SHiP` [48–51], and `MATHUSLA` [33, 37, 48, 52], could be sensitive to mixing angles U^2 close to or even reaching the type-I seesaw predictions $U^2 \sim m_\nu/m_N$, where m_ν denotes the sum of active-neutrino masses and m_N the sterile-neutrino mass, for m_N in the GeV range.

More recently, studies on long-lived HNLs have been extended from minimal to non-minimal scenarios. Sterile neutrinos might only appear sterile at relatively low energies because they interact through some decoupled beyond-the-SM (BSM) particles. Examples are models in which RH neutrinos interact with Z' bosons [53, 54] or leptoquarks [55, 56]. Effective-field-theory (EFT) techniques can efficiently describe such additional interactions. In particular, under the assumption that all BSM fields, except for the sterile neutrinos, are heavy compared to the electroweak scale, the neutrino-extended SM-EFT (νSMEFT) [57–60] Lagrangian describes all interactions between sterile neutrinos and SM fields that are Lorentz- and gauge-invariant. The νSMEFT framework has been used to describe sterile-neutrino phenomenology at a wide range of experiments [48, 61–80].

While efficient, a particular feature of the νSMEFT Lagrangian, which could be a disadvantage from certain perspectives, is that many possible operators exist even when considering operators only up to dimension six. Choosing specific benchmark scenarios where only a few operators are considered simultaneously has become customary. Typically, one operator is selected to allow for the production of a sterile neutrino, while another operator is chosen to induce the sterile neutrino to decay. While straightforward to implement, this procedure oversimplifies the possible underlying BSM scenarios and might not be realistic. In particular, it allows for an effective decoupling between the production and decay of the sterile neutrinos, which is impossible in, for example, the minimal scenario, which we outline below. Similarly, it is possible to consider sterile-neutrino interactions with only very specific quark and lepton flavors, which can altogether avoid the stringent limits from experiments probing lepton number violation such as neutrinoless double beta decay ($0\nu\beta\beta$) searches [81–89]. Again, this might not be very realistic.

JHEP04(2025)007

To alleviate the above-mentioned problem of the νSMEFT, which is rooted in its intrinsic bottom-up approach, one can resort to UV-complete models of non-minimally coupled sterile neutrinos, taking a top-down perspective. In this work, we investigate the minimal left-right symmetric model (mLRSM) [10, 90–94]. In this model, RH neutrinos are charged under an $\mathrm{SU}(2)_R$ gauge symmetry appended to the SM gauge symmetry and interact with so-called RH gauge bosons $W_R^\pm$ and Z'. The mLRSM explains the smallness of the non-vanishing active-neutrino masses with the seesaw mechanism [7–10, 93, 95], provides a dark-matter candidate with the lightest sterile neutrino [96, 97], and interprets the matter-antimatter asymmetry with leptogenesis [98–103]. Limits from collider searches for heavy gauge bosons and light sterile neutrinos indicate that $m_{W_R} \gtrsim 5\,\mathrm{TeV}$ [104, 105] and $Z' \gtrsim 4\,\mathrm{TeV}$ [106], such that the non-minimal interactions of RH neutrinos are feeble, and the nomenclature of sterile neutrinos still applies. While RH neutrinos are often assumed to then also appear at the TeV scale, this is not necessarily true. They could be much lighter, similar to how most SM fermions are light with respect to the electroweak gauge bosons (see ref. [107] for a very recent study on the phenomenology of a light pseudo-Dirac pair of sterile neutrinos in the mLRSM). It has been argued that the relative lightness of RH neutrinos is required to avoid the strong CP problem [108–110]. Furthermore, while the RH interactions of sterile neutrinos are feeble, they can be large compared to the minimal mixing (this is roughly the case if $m_{W_R} < m_W/\sqrt{U} \simeq m_W (m_N/m_\nu)^{1/4} \simeq 30\,\mathrm{TeV}$, for $m_N = 1\,\mathrm{GeV}$ and $m_\nu = 0.05\,\mathrm{eV}$).

This work investigates the phenomenology of the mLRSM with GeV-scale sterile neutrinos.[1] We perform an explicit matching to the νSMEFT framework. We then follow the method of refs. [46, 48] to investigate the discovery potentials for the light long-lived sterile neutrinos with displaced-vertex (DV) searches to be performed at the `LHC` and the near detector of the `DUNE` experiment [113–117] of the Long-Baseline Neutrino Facility (`LBNF`) at Fermilab. For the `LHC`,[2] we focus on the present and future experiments `ANUBIS` [122], `FASER` and `FASER2` [123, 124], `MATHUSLA` [33, 52, 125], `FACET` [126], `CODEX-b` [127], and `MoEDAL-MAPP1` and `MoEDAL-MAPP2` [128, 129], and the recently approved beam-dump experiment `SHiP` [49–51, 130]. Since light sterile neutrinos with RH interactions can significantly impact $0\nu\beta\beta$ rates [131–143], we also make a detailed comparison to complementary probes provided by rare-meson-decay searches and $0\nu\beta\beta$ experiments. Somewhat remarkably, we find that these very different probes have a comparable reach.

This paper is structured as follows. In section 2, we introduce the mLRSM. In section 3, we detail the νSMEFT framework. We discuss sterile-neutrino production and decay in the mLRSM in sections 4 and 5, respectively. We elaborate on the phenomenology of neutrinoless double beta decay in the mLRSM in section 6. In section 7, we explain the numerical simulation and computation procedures for collider analysis based on the theoretical scenarios discussed in the previous sections. We present the numerical results in section 8 and provide our conclusions and an outlook for future work in section 9.

[1] Refs. [111, 112] studied the phenomenology of long-lived sterile neutrinos with masses of order 10-100 GeV in the mLRSM at, respectively, the LHC and lepton colliders.

[2] We omit the `LHC` main experiments `ATLAS` and `CMS`, as their usual trigger requirement of a high-p_T lepton or jet cannot be satisfied for the sterile neutrinos produced from meson decays as considered here. An exception, though, can arise at the `CMS` experiment where specific B-parking datasets [118–120] could be utilized [121], allowing for probing the sterile-neutrino scenarios studied in this work. Nevertheless, since the B-parking searches do not use the full datasets available, we choose not to include this possibility in the work.

JHEP04(2025)007

2 Minimal left-right symmetric model

We provide a concise review of the mLRSM [10, 90–94] in this section. The model extends the electroweak sector of the SM by introducing a gauge-group extension, placing RH fermions into doublets that transform under an $\mathrm{SU}(2)_R$ gauge symmetry. It augments the fermionic particle content of the SM by including RH neutrinos, which are charged under the $\mathrm{SU}(2)_R$ gauge symmetry and couple to $\mathrm{SU}(2)_R$ gauge bosons, known as "RH gauge bosons." In combination with the $\mathrm{SU}(3)_C$ gauge group for the strong interaction, the mLRSM gauge group is given by

$$G_{\mathrm{LR}} \equiv \mathrm{SU}(2)_L \otimes \mathrm{SU}(2)_R \otimes \mathrm{U}(1)_{B-L}, \tag{2.1}$$

where "LR" stands for "left-right", with the associated fermionic particle content

$$(L_{L,R})_i = \begin{pmatrix} \nu_{L,R} \\ \ell_{L,R} \end{pmatrix}_i, \quad (Q_{L,R})_i = \begin{pmatrix} u_{L,R} \\ d_{L,R} \end{pmatrix}_i, \tag{2.2}$$

where $i = 1, 2, 3$ is a generation index, and the L, R subscripts are associated with the left- and right-handed projection operators $P_{L,R} = (1 \mp \gamma_5)/2$. To ensure that the G_{LR} symmetry group breaks down to $G_{\mathrm{SM}} \equiv \mathrm{SU}(2)_L \otimes \mathrm{U}(1)_Y$, the scalar sector in the mLRSM should be an extension of the SM counterpart. To break the G_{LR} gauge symmetry, the following scalar triplets are introduced:

$$\Delta_{L,R} \equiv \begin{pmatrix} \delta^+_{L,R}/\sqrt{2} & \delta^{++}_{L,R} \\ \delta^0_{L,R} & -\delta^+_{L,R}/\sqrt{2} \end{pmatrix}, \tag{2.3}$$

which transform as $\Delta_L \in (\mathbf{3}, \mathbf{1}, 2)$ and $\Delta_R \in (\mathbf{1}, \mathbf{3}, 2)$ under G_{LR}. Furthermore, to govern the breaking of the electroweak symmetry, a scalar bi-doublet is introduced:

$$\Phi \equiv \begin{pmatrix} \phi^0_1 & \phi^+_2 \\ \phi^-_1 & \phi^0_2 \end{pmatrix}, \tag{2.4}$$

which transforms as $\Phi \in (\mathbf{2}, \mathbf{2}^*, 0)$. The Yukawa interactions in the mLRSM are given by

$$\mathcal{L}_Y = -\overline{Q}_L(\Gamma\Phi + \tilde{\Gamma}\tilde{\Phi})Q_R - \overline{L}_L(\Gamma_l\Phi + \tilde{\Gamma}_l\tilde{\Phi})L_R - (\overline{L}^c_L i\sigma_2\Delta_L Y_L L_L + \overline{L}^c_R i\sigma_2\Delta_R Y_R L_R) + \text{h.c.}, \tag{2.5}$$

where $\tilde{\Phi} \equiv \sigma_2\Phi^*\sigma_2$ with σ_2 the second Pauli matrix and $\Gamma, \tilde{\Gamma}, \Gamma_l, \tilde{\Gamma}_l, Y_L$ and Y_R are dimensionless Yukawa coupling matrices. Furthermore, we have defined $\psi^c_{L,R} = P_{R,L}\psi^c$ with $\psi^c \equiv C\overline{\psi}^T$ with the charge conjugation matrix $C = -C^{-1} = -C^\dagger = -C^T$.

We denote the most general form of the scalar fields' vacuum expectation values (vevs) that retain the $\mathrm{U}(1)_{\mathrm{EM}}$ gauge invariance after spontaneous symmetry breaking as

$$\langle\Phi|\Phi\rangle = \begin{pmatrix} \kappa/\sqrt{2} & 0 \\ 0 & \kappa' e^{i\alpha}/\sqrt{2} \end{pmatrix}, \quad \langle\Delta_L|\Delta_L\rangle = \begin{pmatrix} 0 & 0 \\ v_L e^{i\theta_L}/\sqrt{2} & 0 \end{pmatrix}, \quad \langle\Delta_R|\Delta_R\rangle = \begin{pmatrix} 0 & 0 \\ v_R/\sqrt{2} & 0 \end{pmatrix}, \tag{2.6}$$

where all parameters κ, κ', v_L, v_R, α, and θ_L are real-valued [144]. Imposing the relation $\sqrt{\kappa^2 + \kappa'^2} = v$, with $v = 246\,\mathrm{GeV}$ being the electroweak scale, ensures the correct masses

JHEP04(2025)007

for the SM gauge bosons Z and $W^{\pm} \equiv W_L^{\pm}$. Consistency with electroweak precision observables [145] and the absence of right-handed currents in experiments require $v_R \gg v \gg v_L$. The phases α and θ_L induce CP violation, and, as elaborated upon below, the vevs v_L and v_R induce the Majorana neutrino masses.

After the EWSB, the leptonic Yukawa interactions induce the following neutrino-mass terms

$$\mathcal{L}_\nu = \frac{1}{2}\overline{N} M_\nu N^c + \text{h.c.}, \qquad M_\nu = \begin{pmatrix} M_L & M_D \\ M_D^T & M_R \end{pmatrix}, \tag{2.7}$$

where M_ν is a 6×6 symmetric neutrino-mass matrix. We have defined N, which, with the generation index, reads $N_i \equiv (\nu_{Li}, \nu_{Ri}^c)^T$. For the Dirac and Majorana mass matrices, we note the relations

$$M_D \equiv (\kappa \Gamma_l + \kappa' \tilde{\Gamma}_l e^{-i\alpha})/\sqrt{2}, \quad M_L \equiv \sqrt{2} Y_L^\dagger v_L e^{-i\theta_L}, \quad M_R \equiv \sqrt{2} Y_R v_R, \tag{2.8}$$

where, since $v_R \gg v \gg v_L$, one expects $M_R \gg M_D \gg M_L$, although this also depends on the choice of Yukawa couplings.

Throughout this work, it is most convenient to work in the neutrino mass eigenbasis instead of the flavor eigenbasis. For the rotation to the neutrino mass eigenbasis, we follow ref. [133]. Diagonalization of the neutrino mass matrix is achieved through

$$U^\dagger M_\nu U^* = \text{diag}(m_\nu) \equiv (m_1, m_2, m_3, M_4, M_5, M_6), \tag{2.9}$$

where U is a 6×6 unitary matrix. The mass eigenstates $\nu_{1,2,3}$ ($\nu_{4,5,6}$) for the active (sterile) neutrinos can be defined in terms of the current eigenstates as

$$\nu = (\nu_1, \ldots, \nu_6)^T \equiv N_m + N_m^c = \nu^c, \tag{2.10}$$

where we have defined $N \equiv U N_m$ with $N_m \equiv (\nu_L', \nu_R'^c)^T = U^\dagger (\nu_L, \nu_R^c)^T$.

We can express the mixing matrix U as

$$U = \begin{pmatrix} U_{\text{PMNS}} & S \\ T & U_R \end{pmatrix}, \tag{2.11}$$

where U_{PMNS} is the usual 3×3 Pontecorvo-Maki-Nakagawa-Sakata (PMNS) LH neutrino-mixing matrix and U_R its analog for RH neutrinos. The 3×3 matrices S and T dictate the mixing strengths between the left- and right-handed neutrino sectors, which are expressed with

$$S = R U_R, \quad T = -R^\dagger U_{\text{PMNS}}, \tag{2.12}$$

where the 3×3 matrix $R \equiv M_D M_R^{-1}$ generates active-sterile neutrino mixing at the leading order. Also at the leading order, the neutrino-mixing matrices U_{PMNS} and U_R are defined through the relations

$$U_{\text{PMNS}}\, \widehat{m}_\nu\, U_{\text{PMNS}}^T = M_L - M_D M_R^{-1} M_D^T, \tag{2.13}$$

$$U_R \widehat{M}_N\, U_R^T = M_R, \tag{2.14}$$

JHEP04(2025)007

where $\widehat{m}_\nu \equiv \mathrm{diag}(m_1, m_2, m_3)$ and $\widehat{M}_N \equiv \mathrm{diag}(M_4, M_5, M_6)$. For completeness, we note that the PMNS matrix at second order in active-sterile mixing gains non-unitary contributions through $(\mathbf{1} - \eta)U_{\mathrm{PMNS}}$, where $\eta \equiv RR^\dagger/2$. For our purposes, we can safely neglect these contributions since $\eta_{ij} < 10^{-3}$ for every $i, j \in \{e, \mu, \tau\}$ [146].

Suppressing the generation indices, we write the left- and right-handed fields as

$$\nu_L = (PU)P_L\nu = U_{\mathrm{PMNS}}\nu'_L + S\nu'^c_R, \qquad \nu^c_L = (PU^*)P_R\nu = U^*_{\mathrm{PMNS}}\nu'^c_L + S^*\nu'_R \tag{2.15}$$

$$\nu_R = (P_sU^*)P_R\nu = T^*\nu'^c_L + U^*_R\nu'_R, \qquad \nu^c_R = (P_sU)P_L\nu = T\nu'_L + U_R\nu'^c_R. \tag{2.16}$$

Note that, in comparison with the notations used in refs. [147–149], we denote $U_{\mathrm{PMNS}} = V_L$ and $U^*_R = V_R$. In the equations above, the flavor-space projectors P and P_s are 6×3 matrices and defined as

$$P \equiv \left(\mathcal{I}_{3\times3}\ 0_{3\times3}\right), \quad P_s \equiv \left(0_{3\times3}\ \mathcal{I}_{3\times3}\right). \tag{2.17}$$

A main characteristic of the mLRSM is the restoration of parity above v_R. We must impose a discrete symmetry to have an LR symmetry in the Yukawa sector. There are two feasible choices [150]: a generalized charge conjugation ($\mathcal{C}$) or a generalized parity ($\mathcal{P}$) scenario. The discrete field transformations are

$$\mathcal{C}: \quad Q_L \leftrightarrow Q^c_R, \quad L_L \leftrightarrow L^c_R, \quad \Phi \leftrightarrow \Phi^T, \quad \Delta_L \leftrightarrow \Delta^*_R, \tag{2.18}$$

$$\mathcal{P}: \quad Q_L \leftrightarrow Q_R, \quad L_L \leftrightarrow L_R, \quad \Phi \leftrightarrow \Phi^\dagger, \quad \Delta_L \leftrightarrow \Delta_R\,. \tag{2.19}$$

Requiring the Lagrangian to be invariant under these two discrete symmetries respectively leads to the identities

$$\mathcal{C}: \quad M_L = v_L/v_R M_R e^{-i\theta_L}, \quad M_D = M_D^T, \tag{2.20}$$

$$\mathcal{P}: \quad M_L = v_L/v_R M_R^\dagger e^{-i\theta_L}, \quad M_D = M_D^\dagger, \tag{2.21}$$

reducing the number of free parameters. The hermiticity of M_D in the case of $\mathcal{P}$ is only valid in the limit of $(\kappa'/\kappa)\sin\alpha \to 0$ [151, 152].

The spontaneous breaking of the $\mathrm{SU}(2)_L$ and $\mathrm{SU}(2)_R$ leads to massive gauge bosons. For the charged gauge bosons, one expects the $\mathrm{SU}(2)_R$ gauge bosons $W^\pm_R$ to mix with the SM gauge bosons which we label with $W^\pm_L$. The mass eigenstates $W^\pm_{1,2}$ can be rotated into the flavor eigenstates $W^\pm_{L,R}$ through

$$\begin{pmatrix} W^\pm_L \\ W^\pm_R \end{pmatrix} = \begin{pmatrix} \cos\zeta & -e^{\mp i\alpha}\sin\zeta \\ e^{\pm i\alpha}\sin\zeta & \cos\zeta \end{pmatrix} \begin{pmatrix} W^\pm_1 \\ W^\pm_2 \end{pmatrix}, \tag{2.22}$$

where we have defined the mixing parameter

$$\tan\zeta \equiv \frac{g_L\kappa\kappa'}{g_R v_R^2}. \tag{2.23}$$

The physical charged gauge boson masses are

$$M_{W_1} \simeq \frac{g_L v}{2} \simeq M_{W_L}, \quad M_{W_2} \simeq \frac{g_R v_R}{\sqrt{2}} \simeq M_{W_R}, \tag{2.24}$$

JHEP04(2025)007

where $g_{L,R}$ are the $\mathrm{SU}(2)_{L,R}$ gauge couplings, respectively. Once one imposes an LR symmetry, the gauge coupling constants g_L, g_R and the SM $\mathrm{SU}(2)_L$ gauge coupling g become equal, $g = g_L = g_R$ which leads to $M_{W_L}/M_{W_R} \simeq v/(\sqrt{2}v_R) \ll 1$. The above relations result in

$$\zeta \simeq \frac{\xi}{2(\xi^2+1)}\lambda, \quad \text{with } \lambda \equiv \left(\frac{M_{W_L}}{M_{W_R}}\right)^2, \quad \text{and } \xi \equiv \frac{\kappa'}{\kappa}. \tag{2.25}$$

2.1 Seesaw phenomenology

We divide our discussion of the sterile-neutrino phenomenology into canonical type-I and type-II seesaw dominance scenarios. The phenomenology further depends on the choice of the generalized LR symmetry — either imposing the generalized parity $\mathcal{P}$ or the generalized charge conjugation $\mathcal{C}$. We start with the more straightforward type-II seesaw scenario.

2.1.1 Canonical type-II scenario

Dirac Yukawa couplings are assumed to vanish in the canonical type-II seesaw dominance limit, hence $M_D = 0$. This results in a block-diagonal neutrino mass matrix

$$M_N = \begin{pmatrix} M_L & 0 \\ 0 & M_R \end{pmatrix}. \tag{2.26}$$

The physical neutrino masses $\widehat{m}_\nu$ and $\widehat{M}_N$ can be obtained by diagonalizing the Majorana mass matrices M_L and M_R. From eqs. (2.13) and (2.14), we find

$$U_{\mathrm{PMNS}}^\dagger M_L U_{\mathrm{PMNS}}^* = \widehat{m}_\nu, \qquad U_R^\dagger M_R U_R^* = \widehat{M}_N. \tag{2.27}$$

Employing the relations between M_L and M_R given in eqs. (2.20) and (2.21), it is straightforward to obtain the relations between the RH neutrino mixing matrix U_R and the PMNS matrix for the two choices of discrete LR symmetries:

$$\mathcal{C} : U_R = U_{\mathrm{PMNS}} e^{i\theta_L/2}, \qquad \mathcal{P} : U_R = U_{\mathrm{PMNS}}^* e^{-i\theta_L/2}. \tag{2.28}$$

Both of these cases lead to the neutrino mass relation

$$\widehat{M_N} = \frac{v_R}{v_L}\widehat{m}_\nu. \tag{2.29}$$

In the Normal Hierarchy (NH) scenario, we have the active-neutrino mass ordering $m_1 < m_2 < m_3$, with

$$m_{2,3} = (m_1^2 + \Delta m_{21,31}^2)^{1/2}, \tag{2.30}$$

where the squared mass differences $\Delta m_{ij}^2 \equiv m_i^2 - m_j^2$ have been experimentally determined and are tabulated in table 1. On the other hand, the Inverted Hierarchy (IH) scenario has $m_3 < m_1 < m_2$, with

$$m_1 = (m_3^2 + \Delta m_{31}^2)^{1/2}, \quad m_2 = (m_3^2 + \Delta m_{21}^2 - \Delta m_{31}^2)^{1/2}. \tag{2.31}$$

JHEP04(2025)007

	$\Delta m^2_{21}[10^{-5}\ \mathrm{eV}^2]$	$\lvert\Delta m^2_{31}\rvert[10^{-3}\ \mathrm{eV}^2]$	$\sin^2\theta_{12}$	$\sin^2\theta_{23}$	$\sin^2\theta_{13}$	$\delta[^\circ]$
NH	$7.42^{+0.21}_{-0.20}$	$2.514^{+0.027}_{-0.028}$	$0.304^{+0.013}_{-0.012}$	$0.570^{+0.018}_{-0.024}$	$0.02221^{+0.00068}_{-0.00062}$	195^{+51}_{-25}
IH	$7.42^{+0.21}_{-0.20}$	$2.497^{+0.028}_{-0.028}$	$0.304^{+0.013}_{-0.012}$	$0.575^{+0.017}_{-0.021}$	$0.02240^{+0.00062}_{-0.00062}$	286^{+27}_{-32}

Table 1. Active-neutrino oscillation parameters with squared mass differences $\Delta m^2_{ij} \equiv m^2_i - m^2_j$ and $\Delta m^2_{31} > 0$ (< 0) in the NH (IH) [19].

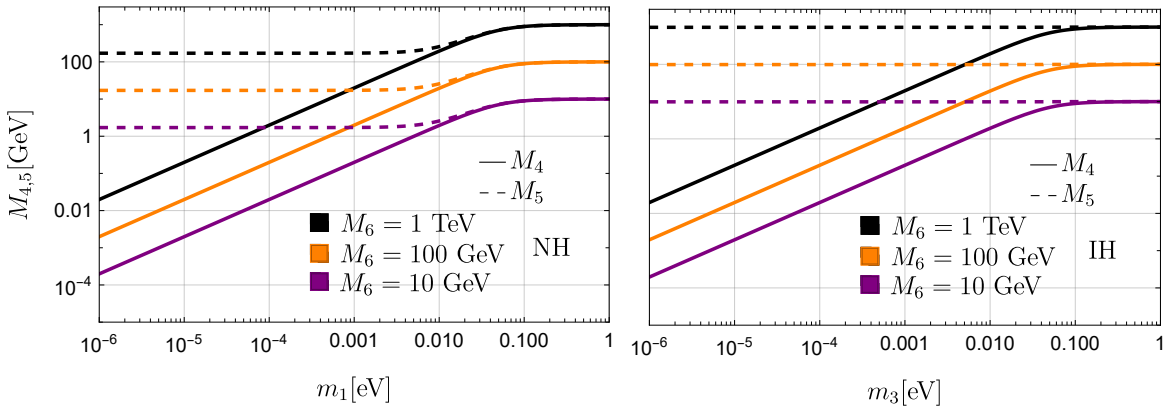

Figure 1. Sterile-neutrino masses M_4 and M_5 as a function of the lightest neutrino mass in both the NH (left) and the IH (right) for different choices of heaviest sterile neutrino mass M_6.

Explicitly, eq. (2.29) implies the relations

$$\mathrm{NH}: M_{4,5} = \frac{m_{1,2}}{m_3} M_6, \qquad \mathrm{IH}: M_{4,5} = \frac{m_{3,1}}{m_2} M_6\,, \tag{2.32}$$

between the active- ($m_{1,2,3}$) and sterile-neutrino mass eigenstates ($M_{4,5,6}$), irrespective of the choice of the additional discrete LR symmetry. The kinematic accessibility of the two lightest sterile neutrinos, $\nu_{4,5}$ with masses $M_{4,5}$, depends on the choice of hierarchy and the choice of m_1 and M_6. The masses of the sterile neutrinos can be expressed in terms of the active-neutrino masses once we fix the highest sterile-neutrino mass and decide the choice of neutrino-mass hierarchy. The relations in eq. (2.32) are depicted in figure 1.

Neutrino-oscillation experiments have measured active-neutrino mixing angles and squared mass differences between the active-neutrino mass eigenstates. We parameterize the PMNS matrix as [153]

$$U_{\mathrm{PMNS}} = \begin{pmatrix} 1 & 0 & 0 \\ 0 & c_{23} & s_{23} \\ 0 & -s_{23} & c_{23} \end{pmatrix} \begin{pmatrix} c_{13} & 0 & s_{13}e^{-i\delta} \\ 0 & 1 & 0 \\ -s_{13}e^{i\delta} & 0 & c_{13} \end{pmatrix} \begin{pmatrix} c_{12} & s_{12} & 0 \\ -s_{12} & c_{12} & 0 \\ 0 & 0 & 1 \end{pmatrix} \begin{pmatrix} 1 & 0 & 0 \\ 0 & e^{i\lambda_1} & 0 \\ 0 & 0 & e^{i\lambda_2} \end{pmatrix}, \tag{2.33}$$

where λ_1 and λ_2 are unknown Majorana phases. We tabulate the current experimental values of these PMNS parameters in table 1.

The decay rates of sterile neutrinos into SM particles — and vice versa — will depend on the sterile-neutrino masses, RH gauge-boson masses, and mixing angles in the diagonalization

JHEP04(2025)007

matrix U; see eq. (2.11). In the generalized parity symmetry $\mathcal{P}$ scenario, a lower limit on the RH gauge-boson masses can be determined through low-energy experimental bounds, independent of the sterile-neutrino masses. In principle, measurements of CP-violation in kaon decays strongly limit $M_{W_R} \geq 17\,\text{TeV}$ [154, 155]. The bound weakens to $M_{W_R} \geq 5.5\,\text{TeV}$ when applying an additional Peccei-Quinn mechanism since additional freedom appears in such a non-trivial model extension. This weaker bound is comparable to limits from direct searches at the LHC [155].

2.1.2 Canonical type-I Scenario

We continue by exploring the mLRSM in the type-I seesaw scenario. In this case, a non-zero Dirac mass matrix M_D is allowed, and the Majorana mass matrix M_L is zero by assuming $v_L = 0$. Unlike the type-II seesaw scenario, sterile-neutrino decay and production rates now gain additional contributions through minimal mixing between the active and sterile neutrinos.

A completely general study of the type-I seesaw scenario is beyond the scope of this work. Instead, we follow ref. [156] and assume an explicit form of the RH neutrino mixing matrix

$$\mathcal{C}: \quad U_R = U_{\text{PMNS}}, \qquad \mathcal{P}: \quad U_R = U^*_{\text{PMNS}}\,. \tag{2.34}$$

In the $v_L = 0$ limit, this leads to the following expressions for the Dirac mass matrix:

$$\mathcal{C}: \quad M_D = U_{\text{PMNS}}\widehat{M}_N\sqrt{-\widehat{M}_N^{-1}\widehat{m}_\nu}U^T_{\text{PMNS}}, \tag{2.35}$$

$$\mathcal{P}: \quad M_D = U_{\text{PMNS}}\widehat{M}_N\sqrt{-\widehat{M}_N^{-1}\widehat{m}_\nu}U^\dagger_{\text{PMNS}}. \tag{2.36}$$

As was the case in the type-II seesaw model, in the limit of $\xi \sin\alpha \to 0$ [151, 152], we obtain the Dirac mass matrix equality in the case of a generalized $\mathcal{P}$ symmetry. To leading order, we can express the active-sterile neutrino mixing matrix $R = M_D M_R^{-1}$ as

$$\mathcal{C}: \quad R = iU_{\text{PMNS}}\widehat{R}U^\dagger_{\text{PMNS}}, \qquad \mathcal{P}: \quad R = iU_{\text{PMNS}}\widehat{R}U^T_{\text{PMNS}}, \tag{2.37}$$

where we have defined

$$\widehat{R} \equiv \text{diag}\left(\sqrt{\frac{m_1}{M_4}}, \sqrt{\frac{m_2}{M_5}}, \sqrt{\frac{m_3}{M_6}}\right). \tag{2.38}$$

Now, we can obtain our final expression for the neutrino mixing matrix U in the type-I Seesaw scenario by substituting eqs. (2.34) and (2.37) into eq. (2.11). For the two choices of LR symmetry, we have

$$\mathcal{C}: \quad U = \begin{pmatrix} U_{\text{PMNS}} & iU_{\text{PMNS}}\widehat{R} \\ iU_{\text{PMNS}}\widehat{R} & U_{\text{PMNS}} \end{pmatrix}, \tag{2.39}$$

$$\mathcal{P}: \quad U = \begin{pmatrix} U_{\text{PMNS}} & iU_{\text{PMNS}}\widehat{R} \\ iU^*_{\text{PMNS}}\widehat{R} & U^*_{\text{PMNS}} \end{pmatrix}, \tag{2.40}$$

which are denoted as $\mathcal{C}$- and $\mathcal{P}$-symmetric, respectively.

JHEP04(2025)007

	Seesaw model	RH neutrino mixing matrix	Relevant parameters
$\mathcal{P}$	Type-I	$U_R = U^*_{\rm PMNS}$	$M_{W_R}, \xi, \alpha, \lambda_1, \lambda_2, \theta_L, m_1, M_4, M_5, M_6$
	Type-II	$U_R = U^*_{\rm PMNS} e^{-i\theta_L/2}$	$M_{W_R}, \xi, \alpha, \lambda_1, \lambda_2, \theta_L, m_1, M_6$
$\mathcal{C}$	Type-I	$U_R = U_{\rm PMNS}$	$M_{W_R}, \xi, \alpha, \lambda_1, \lambda_2, \theta_L, m_1, M_4, M_5, M_6$
	Type-II	$U_R = U_{\rm PMNS} e^{i\theta_L/2}$	$M_{W_R}, \xi, \alpha, \lambda_1, \lambda_2, \theta_L, m_1, M_6$

Table 2. Summary of independent parameters in the mLRSM scenarios under consideration in the NH case. The replacement $m_1 \to m_3$ gives the corresponding summary for the IH case.

It is important to emphasize that, unlike in the type-II seesaw phenomenology, there are no direct relations between the active- and sterile-neutrino masses. Hence, the sterile-neutrino masses $M_{4,5,6}$ are free parameters in the type-I seesaw scenario and could thus vary over a broad mass range. In principle, $M_{4,5,6}$ could all be kinematically allowed in searches for long-lived HNLs. We provide an overview of independent parameters given the seesaw scenarios under consideration in table 2.

3 Standard model effective field theory extended by sterile neutrinos

3.1 The effective neutrino Lagrangian

In the mLRSM, the masses of the RH scalars and gauge bosons depend on the $\mathrm{SU}(2)_R$ vev v_R. However, the sterile neutrinos have masses M_i, with $i = 4, 5, 6$, which we assume to be significantly smaller. Since $M_i \ll v_R$, there is a separation of scales, which suggests applying EFT techniques. At the scale v_R, we integrate out heavy mLRSM degrees of freedom and match to the νSMEFT Lagrangian [60]. The resulting EFT contains singlet ν_R fields in addition to SM fields and accommodates all effective operators explicitly invariant under the SM gauge group.

Since we assume that $v_R \gg v_L$, additional (charged) Higgs scalars are too heavy to contribute to sterile-neutrino production and decay rates significantly. The relevant terms in the charged-current dim-6 νSMEFT Lagrangian containing at least one sterile neutrino are

$$\mathcal{L}^{(6)\rm CC}_{\nu\rm SMEFT} = \sum_i \left\{ C^{(6)}_{\varphi\nu l} \left[(D_\mu \varphi)^\dagger i\tilde{\varphi} \right] \left[\bar{l}^i_R \gamma^\mu \nu^i_R \right] + \sum_{j,k} \left(C^{(6)}_{du\nu l,jk} \left[\bar{u}^j_R \gamma^\mu d^k_R \right] \left[\bar{l}^i_R \gamma_\mu \nu^i_R \right] \right) \right\} + \text{h.c.}, \tag{3.1}$$

where ν_R and l_R are right-chiral neutrino and lepton fields and u_R and d_R are right-chiral up- and down-type quark fields. Furthermore, $i, j, k = \{1, 2, 3\}$ are flavor-generation indices and $C^{(6)}_{du\nu l}, C^{(6)}_{\varphi\nu l}$ are 3×3 matrices in lepton-flavor space that are given by

$$C^{(6)}_{du\nu l,jk} = -\frac{V^R_{jk}}{v_R^2}, \qquad C^{(6)}_{\varphi\nu l} = -\frac{1}{v_R^2} \frac{2\xi}{1+\xi^2} e^{-i\alpha}, \tag{3.2}$$

JHEP04(2025)007

with the ratio of vevs $\xi \equiv \kappa'/\kappa$ (cf. eq. (2.6)) and V_{ij}^R are elements of the RH 3×3 quark-mixing matrix.

In $\mathcal{P}$-symmetric mLRSMs (cf. eq. (2.40)), these are equal to elements of the LH (CKM) quark mixing matrix in the limit of $\xi \sin\alpha \to 0$. In $\mathcal{C}$-symmetric mLRSMs (cf. eq. (2.39)), V^R equals the complex conjugated CKM matrix V^*, up to additional phases. In this work, the amplitudes for meson decays are governed by, at most, one diagram containing one quark transition. Hence, only the norms of the quark mixing matrix elements are relevant, which are equivalent in both the $\mathcal{C}$- and $\mathcal{P}$-symmetric mLRSMs.

After we apply the matching procedure to the νSMEFT Lagrangian, we evolve the higher-dimensional operators to the EW scale v, where we integrate out heavy SM fields (top quark, Higgs boson, and $W^\pm$- and Z-bosons). We match the resulting terms at the tree level to a $\mathrm{SU}(3)_C \otimes \mathrm{U}(1)_{\mathrm{EM}}$-invariant neutrino-extended low-energy EFT (νLEFT). The vector-current operators in eq. (3.1) have vanishing QCD anomalous dimensions at one loop and hence do not evolve under QCD between v_R and v up to negligible electroweak corrections.

The relevant charged-current operators are

$$\begin{aligned}\mathcal{L}^{(6)\mathrm{CC}}_{\nu\mathrm{LEFT}} =& \frac{2G_F}{\sqrt{2}} \sum_{i,j,l} \Bigg\{ \sum_k \Big(\overline{u}^i_L \gamma^\mu d^j_L \left[C^{(6)}_{\mathrm{VLL1},ijkl} \overline{e}^k_L \gamma_\mu \nu^l + C^{(6)}_{\mathrm{VLR1},ijkl} \overline{e}^k_R \gamma_\mu \nu^l \right] \\ &+ C^{(6)}_{\mathrm{VRR},ijkl} \overline{u}^i_R \gamma^\mu d^j_R \overline{e}^k_R \gamma_\mu \nu^l \Big) + \overline{\nu}^i_L \gamma^\mu e^i_L \left[C^{(6)}_{\mathrm{VLL2},jl} \overline{e}^j_L \gamma_\mu \nu^l + C^{(6)}_{\mathrm{VLR2},jl} \overline{e}^j_R \gamma_\mu \nu^l \right] \Bigg\},\end{aligned} \tag{3.3}$$

where we have rotated to the neutrino mass basis, cf. eqs. (2.15) and (2.16). In the equation above, $G_F = (\sqrt{2}v^2)^{-1}$ is the Fermi constant, $u_{L,R}$ and $d_{L,R}$ are chiral up- and down-type quark fields, $e_{L,R}$ are charged lepton fields, and $i, j, k = \{1, 2, 3\}$ are flavor indices, whereas $l = \{1, \ldots, 6\}$ denotes the neutrino mass eigenstates. The Wilson coefficients are given by

$$C^{(6)}_{\mathrm{VLL1},ijkl} = -2V_{ij}(PU)_{kl}, \qquad C^{(6)}_{\mathrm{VLL2},kl} = \frac{C^{(6)}_{\mathrm{VLL1},ijkl}}{V_{ij}}, \tag{3.4}$$

$$C^{(6)}_{\mathrm{VLR1},ijkl} = V_{ij} v^2 (P_s U^*)_{kl}\, C^{(6)}_{\varphi\nu l}, \qquad C^{(6)}_{\mathrm{VLR2},kl} = \frac{C^{(6)}_{\mathrm{VLR1},ijkl}}{V_{ij}}, \tag{3.5}$$

$$C^{(6)}_{\mathrm{VRR},ijkl} = v^2 (P_s U^*)_{kl}\, C^{(6)}_{du\nu l,ij}. \tag{3.6}$$

The relevant neutral-current interactions are

$$\mathcal{L}^{(6)\mathrm{NC}}_{\nu\mathrm{LEFT}} = -\frac{4G_F}{\sqrt{2}} \sum_{i,j,k} \eta_Z^{jk}(f) C^{(6)}_{Z,ijk}(f) \left[\overline{\nu}^j_L \gamma_\mu \nu^i \right] \left[\overline{f}^k \gamma^\mu f^k \right], \tag{3.7}$$

where $i = \{1 \ldots 6\}$ are flavor indices for the neutrino mass eigenstates, $j, k = \{1, 2, 3\}$ are flavor indices for fermion fields $f \in \{u_L, d_L, u_R, d_R, l_L, \nu_L, l_R\}$, and

$$C^{(6)}_{Z,ij}(f) = (PU)_{ji} \left[T^3_L - \sin^2\theta_W Q \right], \tag{3.8}$$

with electric charge Q and the isospin projection $T^3_L = \tau^3/2$ for LH doublets. For the symmetry factor, we have $\eta_Z^{ij}(\nu_L) = \frac{1}{2}(2 - \delta_{ij})$ and $\eta_Z^{ij}(f) = 1$ otherwise.

JHEP04(2025)007

Since the vector-current operators in eq. (3.3) have vanishing QCD anomalous dimensions, they do not evolve between v and sterile-neutrino masses M_i when $v > M_i > \lambda_\chi \sim$ GeV. The dim-6 neutral-current and charged-current νLEFT Lagrangians are sufficient to calculate all sterile-neutrino production and decay rates in this work.

All the terms in the dim-6 νLEFT Lagrangian are lepton-number conserving. Nevertheless, they allow for non-zero contributions to $0\nu\beta\beta$ processes, which induce lepton-number violation through Majorana masses M_i originating from virtual neutrino propagators. We further elaborate on this point in section 6.

4 Sterile-neutrino production

In this section, we investigate the production rates of sterile neutrinos. We focus on the production via decays of mesons, which are copiously produced at the interaction points (IPs) of the experiments considered in this work. The production of sterile neutrinos with mass $\mathcal{O}$(GeV) via the decays of Higgs, W- and Z-boson, if existent, is subdominant as a result of the relatively smaller production cross sections of these bosons, and is hence not considered here. This analysis studies leptonic and semi-leptonic decays of $K^\pm$, K_L, K_S, $D^\pm, D^0, D_s, B^\pm, B^0$, and B_s mesons. We neglect subdominant contributions from B_c, J/Ψ, and Υ mesons, though they might extend the upper mass reach of the sterile neutrinos to a minor extent.

4.1 Minimal mixing scenario

We start by analyzing the phenomenology of a scenario where sterile neutrinos are only produced through minimal mixing with the SM neutrinos. In this scenario, there are no RH gauge-boson contributions, and the production of the sterile neutrinos occurs exclusively via LH currents. The only relevant Wilson coefficients are $C^{(6)}_{\mathrm{VLL1},ijkl} = -2V_{ij}(PU)_{kl}$, where V_{ij} are CKM matrix elements and U the neutrino mixing matrix.

It is simplest to assume that only the lightest sterile neutrino is kinematically available to be produced from the meson decays. From this point forward, for notational clarity, we will denote the sterile neutrino mass eigenstates as N_4, N_5 and N_6. The sterile-neutrino mass range we consider is $0 < M_4 < m_{B_s} \sim 5.37$ GeV. Unless explicitly stated otherwise, we follow ref. [156] for our decay-rate calculations, including the phase-space integration, the relevant form-factor parameterizations, and the decay constants.

We consider the branching ratios of mesons decaying into final states that include exactly one sterile neutrino. This is reasonable in the minimal mixing scenario owing to the smallness of the relevant neutrino mixing angles. Branching ratios in this scenario have been calculated and discussed extensively in the literature; see e.g. refs. [26, 156]. In the considered sterile-neutrino production processes, either no meson, a pseudoscalar meson, or a vector meson accompanies the sterile neutrino in the final state.

In figure 2, the branching ratios of $B, D \to e^- + N_4 + X$ processes are shown for mixing angles $(U_{e4}, U_{\mu 4}, U_{\tau 4}) = (1, 0, 0)$, where X denotes the potential final-state meson. We have arbitrarily set the mixing angle $U_{e4} = 1$ since the decay rates in all depicted processes scale with an overall factor $|U_{e4}|^2$. From figure 2, it is evident that decays with no mesons, pseudoscalar mesons, or vector mesons in the final-state configuration all give dominant contributions at different points in the sterile-neutrino mass range. Hence, we take all

JHEP04(2025)007

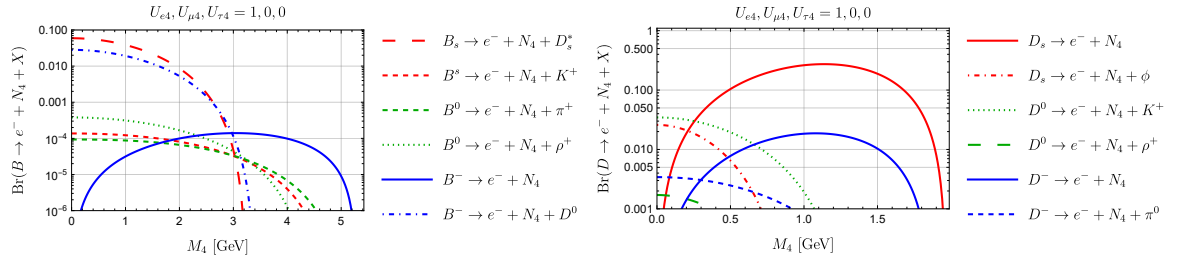

Figure 2. A selection of branching ratios for decays of B and D mesons into a sterile neutrino in the minimal scenario.

these decays into account in our further analysis. Our results agree with those derived in previous works [26, 48].

4.2 Left-right symmetric models

We continue by analyzing sterile-neutrino production in the mLRSM scenarios. We first assume a type-II seesaw scenario, where Dirac masses M_D are set to zero, and there is no minimal mixing between the left- and right-handed neutrino sectors. Hence, all active-sterile neutrino mixing angles are zero, and there are no purely LH current interactions with sterile neutrinos since $C^{(6)}_{\mathrm{VLL1}} = 0$. Neutral-current sterile-neutrino production via semi-leptonic meson decays is loop-suppressed because the Z and Z' boson interactions are quark-flavor diagonal. An example of such a decay would be $B_s \to K_S/\phi + N_{4,5} + N_{4,5}$. Because of this loop suppression, such decay channels are neglected. This implies that the right-handed charged gauge boson W_R is the only BSM gauge boson providing non-negligible contributions to the meson decay rates.

Since we neglect neutral-current processes, the sterile-neutrino production rates are similar for all sterile-neutrino mass eigenstates with identical masses. That is, in this limit, the only difference between the production rates of N_4, N_5, and N_6 via meson decays arises from an overall factor $|U_R|^2_{kl}$ containing the appropriate RH neutrino mixing-matrix angle. This implies

$$\frac{\mathrm{Br}(M \to \ell^- + N_{k_1} + X)}{\mathrm{Br}(M \to \ell^- + N_{k_2} + X)} = \frac{|U_R|^2_{k_1 l}}{|U_R|^2_{k_2 l}}, \tag{4.1}$$

where the meson $M \in \{B, D, K\}$ and the charged lepton $\ell \in \{e, \mu, \tau\}$. Since only the absolute squares of the mixing angles are relevant, there is no dependence on the complex phases λ_1, λ_2, and θ_L that appear in U_R. The choice of the discrete LR symmetry is also irrelevant to the meson decay rates in this scenario. This greatly simplifies the available parameter space. The choice of the heaviest neutrino mass, M_6, fixes the mass relation between the active-neutrino mass m_1 and the lightest sterile neutrino mass M_4 and does not impact the meson decay rates as long as M_6 is large enough to make N_5 kinematically unavailable, cf. eq. (2.32). For simplicity, we set the CP-violating phase $\alpha = 0$. From table 2, in the limit where only N_4 is kinematically available, it is then apparent that only two relevant benchmark parameters remain. These are the $\xi = \kappa'/\kappa$, which determines the W_L-W_R mixing strength, and M_{W_R}, which is the mass of the RH charged gauge boson.

JHEP04(2025)007

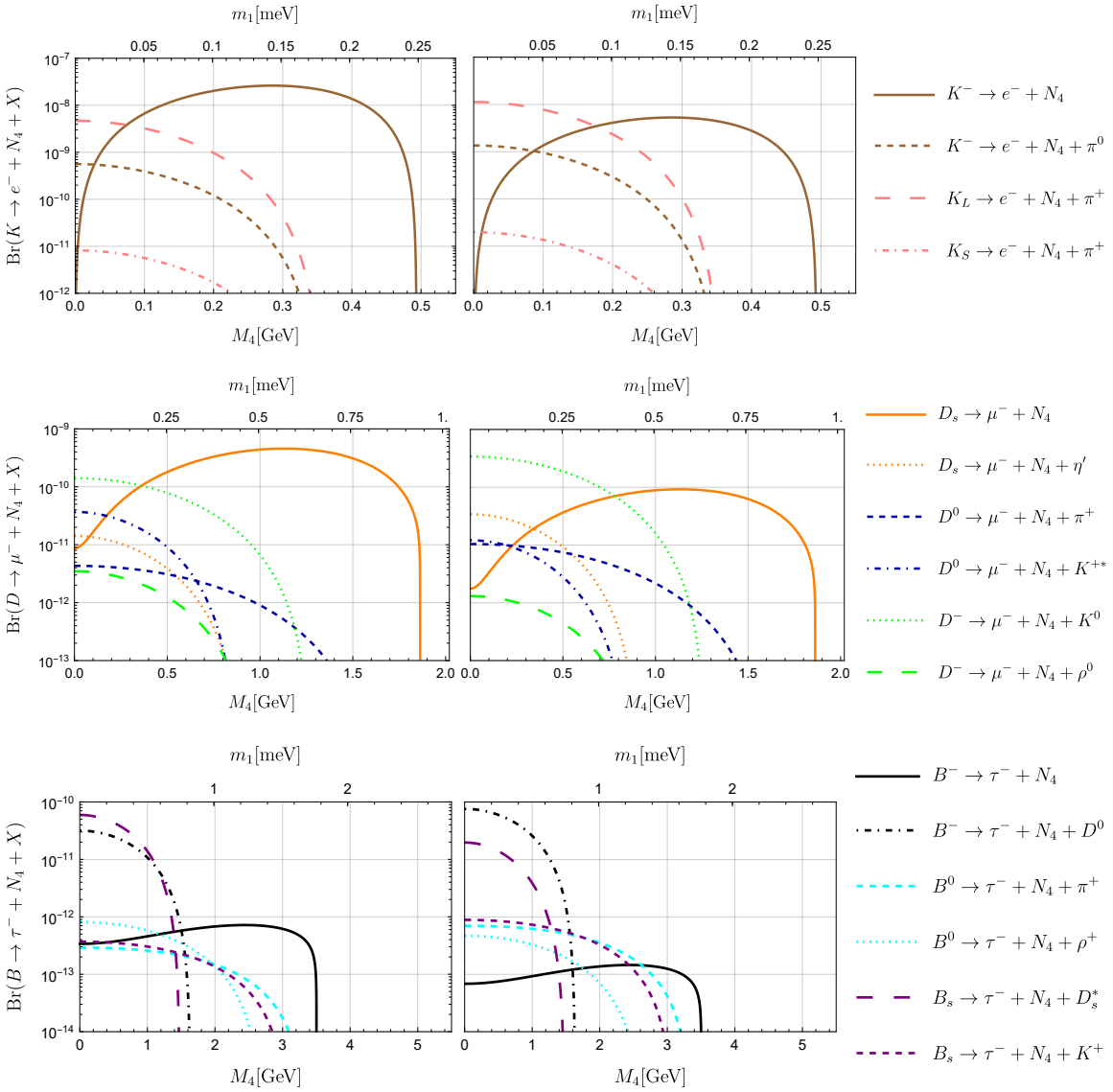

Figure 3. A selection of branching ratios for $M \to l^- + N_4 + X$ decay processes, where $M = \{B, D, K\}$ and $l = \{e, \mu, \tau\}$, in mLRSM scenarios for $M_6 = 100\,\mathrm{GeV}$ and $M_{W_R} = 7\,\mathrm{TeV}$. We work in the NH and have set the W_L-W_R mixing parameter $\xi = 0$ ($\xi = 0.3$) in the left (right) panels.

In figure 3, representative branching ratios are shown for $M \to \ell^- + N_4 + X$ decay processes. We have fixed the RH gauge-boson mass at a relatively small value of $M_{W_R} = 7\,\mathrm{TeV}$ and considered both cases of $\xi = 0$ and $\xi = 0.3$ for the W_L-W_R mixing parameter. In this scenario, all decay rates that produce sterile neutrinos scale with $M_{W_R}^{-4}$. The heaviest sterile-neutrino mass has been set to $M_6 = 100\,\mathrm{GeV}$, so the sterile-neutrino mass eigenstate M_5 is kinematically unavailable. Choosing a larger value for M_6 would not impact the dependence of the meson decay rates on M_4, but it would shift the m_1 axes through eq. (2.32). Leptonic and semi-leptonic meson decays into final-state pseudoscalar or vector mesons dominate the sterile-neutrino production rates at different M_4 and are hence all considered in the further analysis.

JHEP04(2025)007

Furthermore, a non-zero value of ξ amplifies the pseudoscalar-meson decay rates into a sterile neutrino, a charged lepton, and a pseudoscalar meson. In contrast, $\xi \neq 0$ suppresses pseudoscalar-meson two-body decays, and pseudoscalar-meson decays into a sterile neutrino, a charged lepton, and a vector meson. The interference terms in the meson decay rates between the Wilson coefficients $C^{(6)}_{\mathrm{VRR}}$ and $C^{(6)}_{\mathrm{VLR}}$ that appear for $\xi \neq 0$ cause these effects. For semi-leptonic B- and D-meson decays, the relevant hadronic matrix elements are

$$\langle h_{\mathrm{PS}}|\,\overline{q}_1\gamma^\mu P_{L,R} q_2\,|B,D\rangle = +\frac{1}{2}\,\langle h_{\mathrm{PS}}|\,\overline{q}_1\gamma^\mu q_2\,|B,D\rangle\,, \tag{4.2}$$

$$\langle h_{\mathrm{V}}|\,\overline{q}_1\gamma^\mu P_{L,R} q_2\,|B,D\rangle = \mp\frac{1}{2}\,\langle h_{\mathrm{V}}|\,\overline{q}_1\gamma^\mu\gamma^5 q_2\,|B,D\rangle\,, \tag{4.3}$$

where h_{PS} and h_V are pseudoscalar mesons and vector mesons, respectively, and the minus (plus) sign on the right-hand side of eq. (4.3) corresponds to the projection operator P_L (P_R). This relative minus sign in eq. (4.3) — which also appears in the two-body leptonic decays — leads to destructive interference terms linear in ξ. These effects are sizable for large ξ. Explicitly, the decay rates will be proportional to a factor $|C^{(6)}_{\mathrm{VRR}} \mp C^{(6)}_{\mathrm{VLR1}}|^2$. In the limit where the CP-violating phase $\alpha = 0$, we have $C^{(6)}_{\mathrm{VLR1}} = \frac{2\xi}{1+\xi^2} C^{(6)}_{\mathrm{VRR}}$, cf. eqs. (3.2), (3.5) and (3.6). Hence, for values of ξ approaching 1, the three-body decays into a pseudoscalar meson, and the two-body leptonic decays are suppressed.

In type-I seesaw scenarios, sterile-neutrino production can occur via contributions from active-sterile neutrino mixing *and* RH currents. In the vanishing W_L-W_R mixing limit, one can analytically determine under what conditions contributions from either the RH current or the active-sterile mixing dominate the meson-decay processes. If only the lightest sterile neutrino N_4 is kinematically available, both contributions are equivalent when

$$\left(\frac{M_{W_R}}{80\ \mathrm{TeV}}\right)^4 \left(\frac{m_1}{\mathrm{meV}}\right) \left(\frac{\mathrm{GeV}}{M_4}\right) \simeq 1\,. \tag{4.4}$$

For instance, given the lightest sterile neutrino at the pion threshold ($M_4 = 0.14\,\mathrm{GeV}$), the RH-current contributions will dominate for $M_{W_R} \leq 50\,\mathrm{TeV}$ if $m_1 = 1$ meV. Employing the relation above, we see that for relatively light $M_{W_R} < 10\,\mathrm{TeV}$ and $\xi = 0$, type-I seesaw scenarios converge to type-II scenarios since the minimal-mixing contributions are negligible for every reasonable choice of the lightest active-neutrino mass[3] in the sterile-neutrino mass range $m_\pi < M_4 < m_{B_s}$.

5 Sterile-neutrino decay

In this section, we study the leptonic and semi-leptonic decays of sterile neutrinos. The leptonic decays may proceed via charged or neutral weak currents. For the sterile-neutrino decays into mesons, we consider the pseudoscalar mesons ($\pi, K, \eta, \eta', D, D_s, \eta_c$) and the vector mesons ($\rho, \omega, K^*, \phi, D^*, D_s^*$). We employ the physical parameters, decay constants, and form factors listed in ref. [48] to compute the relevant decay processes.

The decays into multi-meson final states warrant some discussion. As argued in ref. [26], these become relevant for sterile neutrinos heavier than roughly 1 GeV in the minimal

[3]This requires $\sum_{i=1,2,3} m_i < 0.12\,\mathrm{eV}$, considering cosmological constraints [157–161].

JHEP04(2025)007

case. In the previous work, to avoid the tedious process of summing exclusive multi-meson decay channels, the contributions of multi-meson final states have been approximated by multiplying the decay width of sterile neutrinos into spectator quarks with an appropriate loop correction [162–164], which was initially employed to calculate multi-meson corrections in inclusive hadronic decay rates of the τ lepton. We employ this procedure here as well for the minimal scenario. For sterile neutrinos with masses below 1 GeV, we compute the lifetimes by explicitly summing over final states that are purely leptonic or contain a single meson [26, 48], while for masses above 1 GeV, we use

$$\Gamma(N_4 \to \ell^-/\nu_\ell + \text{hadrons}) \simeq [1 + \Delta_{\text{QCD}}(M_4)]\, \Gamma_{\text{tree}}(N_4 \to \ell^-/\nu_\ell + \overline{q_1} q_2), \tag{5.1}$$

where

$$\Delta_{\text{QCD}}(M_4) = \frac{\alpha_s(M_4)}{\pi} + 5.5\frac{\alpha_s(M_4)^2}{\pi^2} + 26.4\frac{\alpha_s(M_4)^3}{\pi^3}\,. \tag{5.2}$$

5.1 Left-right symmetric models

In mLRSM scenarios, determining the precision of the multi-meson corrections is more subtle. In a type-II seesaw scenario without W_L-W_R mixing, all mesons produced in sterile-neutrino decays couple to $W_R^\pm$ gauge bosons, whereas in the minimal scenario, they couple to $W_L^\pm$ gauge bosons. Since QCD is invariant under parity transformations, we expect the multi-meson corrections to hold similarly in these scenarios. In this case, employing eq. (5.1) would be appropriate for sterile-neutrino masses above 1 GeV. In principle, this is no longer true once we consider non-zero W_L-W_R mixing scenarios since the ξ dependence is dictated by the parity of the hadronic final state [in analogy to eqs. (4.2) and (4.3)]. Because $\xi < 0.8$ cannot be too large in practice [150], we neglect this difference and use eq. (5.1) also when including W_L-W_R mixing. We do not expect this approximation to significantly affect our results, but we stress that explicitly computing the QCD corrections would be interesting for accounting for these W_L-W_R mixing effects.

In figure 4, we compare single-meson and multi-meson decay widths by naively applying the inclusive hadronic corrections in a scenario where $\xi = 0.3$. The naive corrections appear significant for $M_4 > 1.55\,\text{GeV}$, and assuming single-meson currents, as shown in the plot, leads to a systematic underestimate of the hadronic contributions to sterile-neutrino decays. Hence, for $\xi = 0.3$, we calculate the total sterile-neutrino decay rates in this scenario by applying eq. (5.1) for $1.55\ \text{GeV} < M_4 < m_{B_s}$. One can straightforwardly generalize this approach for different values of ξ.

Figure 5 depicts the proper decay length of the lightest sterile neutrino $c\tau_{N_4}$ for type-II seesaw scenarios with and without W_L-W_R mixing, where c is the speed of light and τ_{N_4} is the proper lifetime of the sterile neutrino. Working in the NH — which is what we will do throughout this work — we consider a scenario with $M_{W_R} = 7\,\text{TeV}$, $M_6 = 100\,\text{GeV}$ such that N_5 is kinematically unavailable, and $\xi = 0.3$. It is perhaps surprising that around $M_4 = 1\,\text{GeV}$, the N_4 lifetimes are nearly equal despite the substantial interference effects caused by the non-zero W_L-W_R mixing, but this is partially the case because we apply the same naive inclusive hadronic correction in both cases. These decay lengths allow for the detection of sterile neutrinos in prospective far-detector experiments at the LHC, as well as at DUNE, and SHiP. We discuss this further in section 7.

JHEP04(2025)007

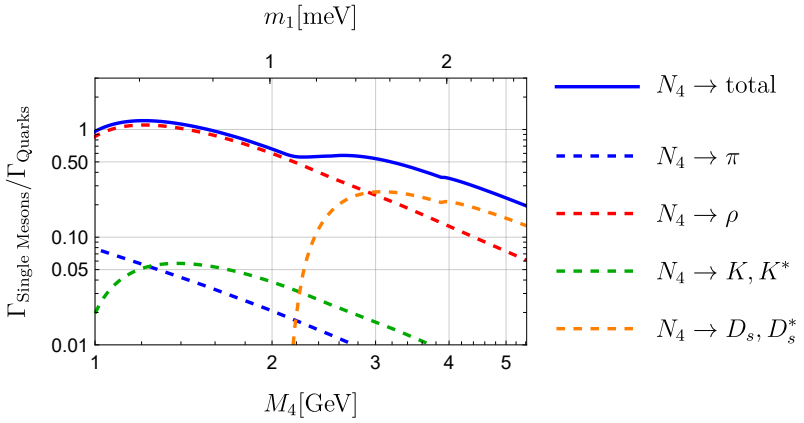

Figure 4. Ratios of the sterile-neutrino decay widths into individual mesons to the inclusive hadronic decay width calculated with eq. (5.1) for $\xi = 0.3$ and $M_6 = 100\,\text{GeV}$, as functions of M_4/m_1. The solid line labeled with "$N_4 \to$ total" corresponds to the sum of the dashed curves.

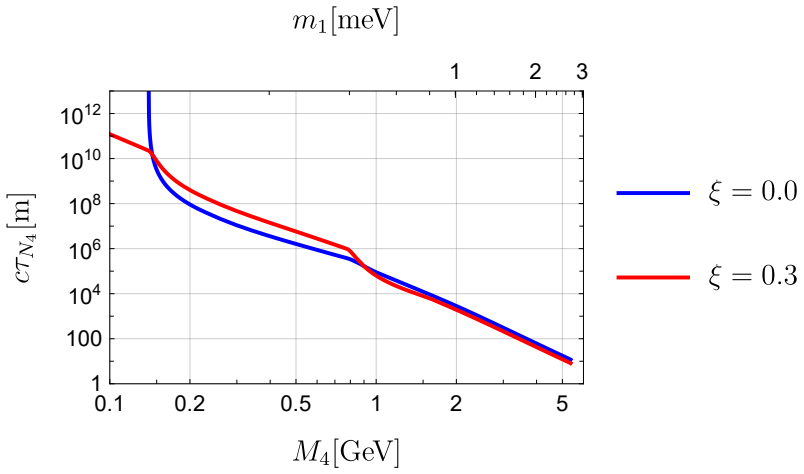

Figure 5. Proper decay lengths of sterile neutrinos in type-II seesaw mLRSM scenarios with and without W_L-W_R mixing for $M_{W_R} = 7\,\text{TeV}$ and $M_6 = 100\,\text{GeV}$.

In figure 6, the primary decay branching ratios of the lightest sterile neutrino N_4 into SM leptons and bound-state mesons are depicted for $M_4 < 1.55\,\text{GeV}$. The hadronic decays dominate the sterile-neutrino decay processes once they become kinematically accessible around the charged pion threshold $M_4 > M_{\pi^\pm} = 139.6\,\text{MeV}$. The vector meson $N_4 \to e^-/\mu^- + \rho^+$ decay modes dominate at larger M_4, which is unsurprising as a result of the constructive interference terms in the decay rates being linear in ξ and the fact that these processes are Cabibbo-allowed. These branching fractions are independent of the charged RH gauge-boson mass M_{W_R} since all decay rates scale as $M_{W_R}^{-4}$.

In figure 7, the proper decay lengths for the lightest sterile neutrino N_4 as functions of M_4 are shown in type-I seesaw scenarios without W_L-W_R mixing for various values of the lightest active neutrino's mass m_1 and the RH gauge boson's mass M_{W_R}. The maximum value $m_1 = 3 \times 10^{-2}\,\text{eV}$ is close to the upper limit permissible under the cosmological constraints

JHEP04(2025)007

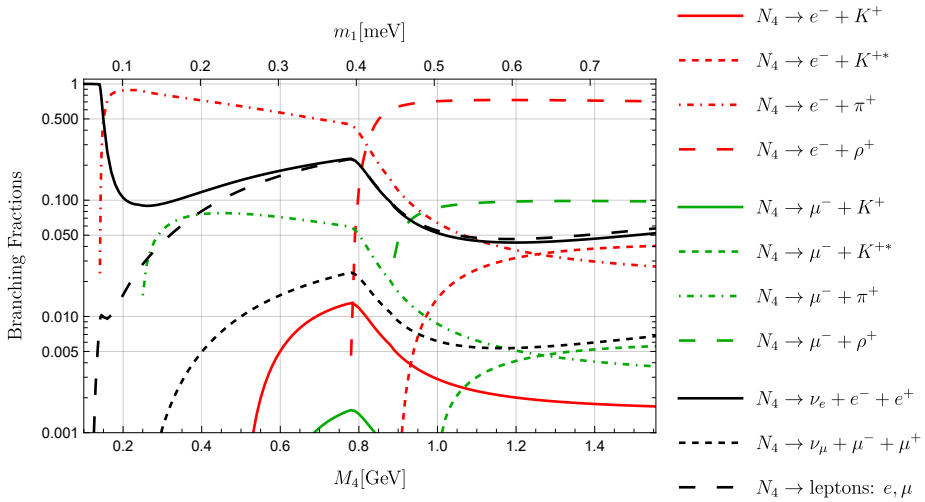

Figure 6. Sterile-neutrino decay branching fractions in a type-II seesaw mLRSM scenario where $\xi = 0.3$ and $M_6 = 100\,\text{GeV}$. The $N_4 \to \text{leptons} + e, \mu$ branching fraction includes every N_4 decay mode that includes one electron and one muon.

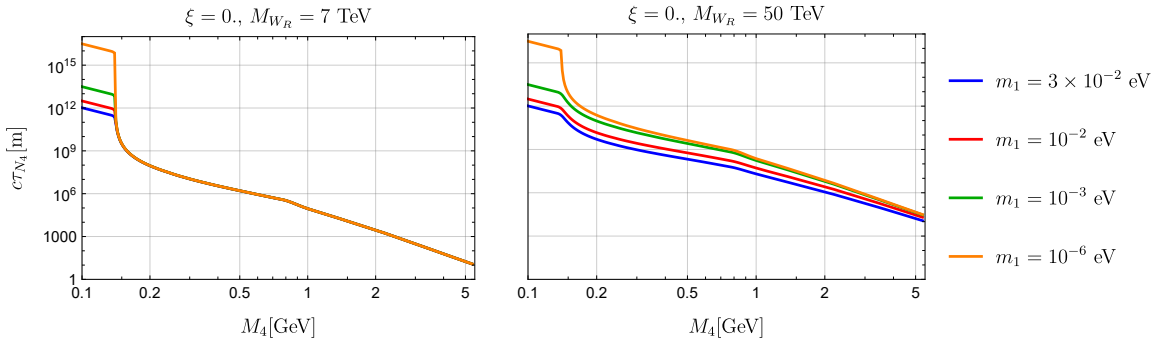

Figure 7. Proper decay lengths of the lightest sterile neutrino in type-I seesaw scenarios for several values of m_1 and M_{W_R}, with $\xi = 0$.

on the active-neutrino masses [157–161]. The left (right) panel shows the scenario where $M_{W_R} = 7\,\text{TeV}$ (50 TeV). For $M_{W_R} = 7\,\text{TeV}$, when the sterile-neutrino mass surpasses the charged-pion threshold, and RH currents start contributing to the sterile-neutrino decays, the dependence of the sterile-neutrino lifetime on the lightest sterile-neutrino mass immediately diminishes. This is due to the relatively light mass of the charged RH gauge boson. For $M_4 < M_{\pi^\pm}$, the only kinematically available decay channels are neutral-current decays, which depend linearly on m_1. In contrast, the sterile-neutrino lifetimes for $M_{W_R} = 50\,\text{TeV}$ exhibit a more substantial dependence on m_1 across the relevant M_4 mass range. This dependence becomes progressively less significant as M_4 increases. The proper-lifetime behavior is similar in a scenario where $\xi = 0.3$.

JHEP04(2025)007

6 Neutrinoless double beta decay

Neutrinos being Majorana states and lepton number violation are key features of the mLRSM. These features lead to non-zero $0\nu\beta\beta$ decay rates. In addition to the usual contributions arising from the exchange of light active neutrinos between two nucleons in a nucleus, interesting additional contributions appear in the mLRSM.

First of all, with just LH weak interactions, additional contributions arise from the exchange of the heavier sterile neutrinos as a result of the mixing between ν_L and ν_R. Then, in the mLRSM, owing to the RH gauge interactions, there are contributions solely from ν_R exchange. The W_L-W_R mixing also leads to additional topologies. Further, there can be diagrams involving minimal mixing and right-handed gauge interactions (sometimes these are called the λ and η mechanisms [165]). Finally, there are contributions from the exchange of the doubly charged scalars $\delta^{++}_{L,R}$. However, in scenarios with relatively light RH neutrinos, these contributions are sub-leading and can be neglected [156]. Which of these contributions dominates depends on the interplay between the sterile-neutrino masses, the M_{W_L}/M_{W_R} mass ratio, and the amount of W_L-W_R mixing.

The various contributions to $0\nu\beta\beta$ decays in the mLRSM have been investigated in different approaches [165–169]. In the last years, significant progress has been made towards a systematic EFT description of the $0\nu\beta\beta$ decays that takes into account the large-scale separations between the lepton-number-violating mechanism, the typical scale of nuclear physics, and the energy release in the $0\nu\beta\beta$ decays [170–174]. This framework has been used to compute the $0\nu\beta\beta$ decay rates within the mLRSM. The formulae are rather lengthy and explicitly given in ref. [156]. Here, we discuss the salient features.

Within the mLRSM, the $0\nu\beta\beta$ decay amplitude mainly depends on two structures[4]

$$\mathcal{A} = \frac{g_A^2 G_F^2 m_e}{\pi R_A}\left[\sum_{i=1}^{6}\mathcal{A}_L(m_i)\,\bar{e}(k_1)P_R e^c(k_2) + \sum_{i=1}^{6}\mathcal{A}_R(m_i)\,\bar{e}(k_1)P_L e^c(k_2)\right] + \dots\,, \tag{6.1}$$

where $g_A \simeq 1.27$ is the nucleon axial charge and $R_A \simeq 1.2\,A^{1/3}\,\text{fm}$ is the nuclear radius of a nucleus with A nucleons. The dots denote other structures that are sub-leading [156]. After integrating over the final state phase space, the $0\nu\beta\beta$ decay rate is then given by

$$\left(T^{0\nu}_{1/2}\right)^{-1} = g_A^4\left[G_{01}\left(|\mathcal{A}_L|^2 + |\mathcal{A}_R|^2\right) - 2(G_{01}-G_{04})\text{Re}\mathcal{A}_L^*\mathcal{A}_R\right]\,, \tag{6.2}$$

where $\mathcal{A}_{L,R} = \sum_{i=1}^{6}\mathcal{A}_{L,R}(m_i)$ and $G_{01,04}$ are atomic phase-space factors. We will consider ^{136}Xe for which $\{G_{01},\,G_{04}\} = \{1.5,\,3.2\}\cdot 10^{-14}\,\text{yr}^{-1}$.

The structure $A_L(m_i)$ involves the LH charged leptonic current and includes the exchange of the active Majorana neutrinos. The relevant expression is given by

$$\mathcal{A}_L(m_i) = -\frac{m_i}{4m_e}\mathcal{M}(m_i)\,\left(C^{(6)}_{\text{VLL}}\right)^2_{udei}\,, \tag{6.3}$$

in terms of the nuclear matrix element (NME) $\mathcal{M}(m_i)$, that depends on the mass of the exchanged neutrino (technically, it is a combination of hadronic and nuclear matrix elements, but we use NME here for simplicity). In the modern approach, the NMEs are computed by

[4] In this section we sometimes use for notational convenience $m_{1,2,3,4,5,6}$ instead of $m_{1,2,3}$ and $M_{4,5,6}$.

JHEP04(2025)007

combining chiral EFT with many-body nuclear methods. For a detailed discussion of the mass dependence of the NMEs, we refer to refs. [76, 143, 175].

We recall that in the mLRSM $(C^{(6)}_{\rm VLL})_{udei} = -2V_{ud}(PU)_{ei}$. In the type-II seesaw limit, the 6×6 U-matrix is block-diagonal, and the LH amplitude only sums over the active neutrinos. In this case, we can neglect the neutrino-mass dependence of the NMEs and obtain

$$\mathcal{A}_L \simeq -\frac{V_{ud}^2}{m_e}\mathcal{M}(0)\sum_{i=1}^{3}(U_{\rm PMNS})_{ei}^2\, m_i \equiv -\frac{V_{ud}^2}{m_e}\mathcal{M}(0)\, m_{\beta\beta}\,, \tag{6.4}$$

in terms of the effective Majorana neutrino mass $m_{\beta\beta}$ and $\mathcal{M}(0) = \mathcal{O}(1)$. Beyond the type-II limit, $\mathcal{A}_L(m_i)$ generally depends on the exchange of sterile neutrinos.

The second structure $A_R(m_i)$ involves RH charged lepton currents. Within the mLRSM, it consists of two contributions

$$\mathcal{A}_R(m_i) = -\frac{m_i}{4m_e}\left[\mathcal{M}(m_i)\,\left(C^{(6)}_{\rm VRR} + C^{(6)}_{\rm VLR}\right)^2_{udei} + 2\mathcal{M}_{LR}(m_i)\,\left(C^{(6)}_{\rm VRR}\right)_{udei}\left(C^{(6)}_{\rm VLR}\right)_{udei}\right]. \tag{6.5}$$

The first term corresponds to two RH charged quark currents. Because QCD conserves parity, the associated NME is the same as in eq. (6.3). The second term involves both a left- and a right-handed charged quark current and comes with its own NME.

In the type-II limit and turning off W_L-W_R mixing (setting $\xi = 0$ and thus $C^{(6)}_{\rm VLR} = 0$), we obtain

$$\mathcal{A}_R^{\xi=0} \simeq -\frac{V_{ud}^2}{m_e}\frac{M_{W_L}^4}{M_{W_R}^4}\sum_{i=4}^{6}\mathcal{M}(M_i)\,(U_{\rm PMNS})_{eI}^2\; M_i\,, \tag{6.6}$$

where $I \equiv i-3$. We can now compare the RH contributions to the standard LH contributions in eq. (6.3). For very light sterile neutrinos $M_{4,5,6} \ll m_\pi$ (not the focus of this work), we can again neglect the neutrino mass in the NME and obtain

$$\frac{\mathcal{A}_R^{\xi=0}}{\mathcal{A}_L} \sim \frac{M_{W_L}^4}{M_{W_R}^4}\frac{M_{\beta\beta}}{m_{\beta\beta}} \simeq (4\cdot 10^3)\left(\frac{1\,\text{TeV}}{M_{W_R}}\right)^4\left(\frac{0.01\,\text{eV}}{m_{\beta\beta}}\right)\left(\frac{M_{\beta\beta}}{1\,\text{MeV}}\right), \tag{6.7}$$

where $M_{\beta\beta} \equiv \sum_{i=4}^{6}(U_{\rm PMNS})_{eI}^2\, M_i$. For example, for $M_{\beta\beta} \simeq 1\,\text{MeV}$ and $m_{\beta\beta} \simeq 0.1\,\text{eV}$, RH contributions dominate for $M_{W_R} \leq 8\,\text{TeV}$.

In the opposite limit $M_{4,5,6} \gg m_\pi$, we have $\mathcal{M}(M_i) \sim m_\pi^2/M_i^2$ so that A_R is dominated by the lightest sterile neutrino M_4. In this limit, we have roughly

$$\frac{\mathcal{A}_R^{\xi=0}}{\mathcal{A}_L} \sim \frac{M_{W_L}^4}{M_{W_R}^4}\frac{m_\pi^2}{m_{\beta\beta}M_4} \simeq (8\cdot 10^4)\left(\frac{1\,\text{TeV}}{M_{W_R}}\right)^4\left(\frac{0.01\,\text{eV}}{m_{\beta\beta}}\right)\left(\frac{1\,\text{GeV}}{M_4}\right). \tag{6.8}$$

For $M_4 = 1\,\text{GeV} \ll M_{5,6}$ and $m_{\beta\beta} = 0.1\,\text{eV}$, the RH contributions dominate for $M_{W_R} \leq 20\,\text{TeV}$. While these expressions are only estimates, they give an idea of the scale that can be reached.

The situation becomes more complicated and interesting once we turn on W_L-W_R mixing. This leads to a non-zero value of $C_{\rm VLR}$ and an additional contribution to $\mathcal{A}_R$. In the type-II limit, we can write

$$\mathcal{A}_R^{\xi} \simeq \mathcal{A}^{\xi=0}\left[1 + \frac{4\xi^2}{(1+\xi^2)^2}e^{-2i\alpha}\right] - \frac{V_{ud}^2}{m_e}\frac{M_{W_L}^4}{M_{W_R}^4}\frac{4\xi e^{-i\alpha}}{1+\xi^2}\sum_{i=4}^{6}\mathcal{M}_{LR}(M_i)\,(U_{\rm PMNS})_{eI}^2\; M_i\,. \tag{6.9}$$

JHEP04(2025)007

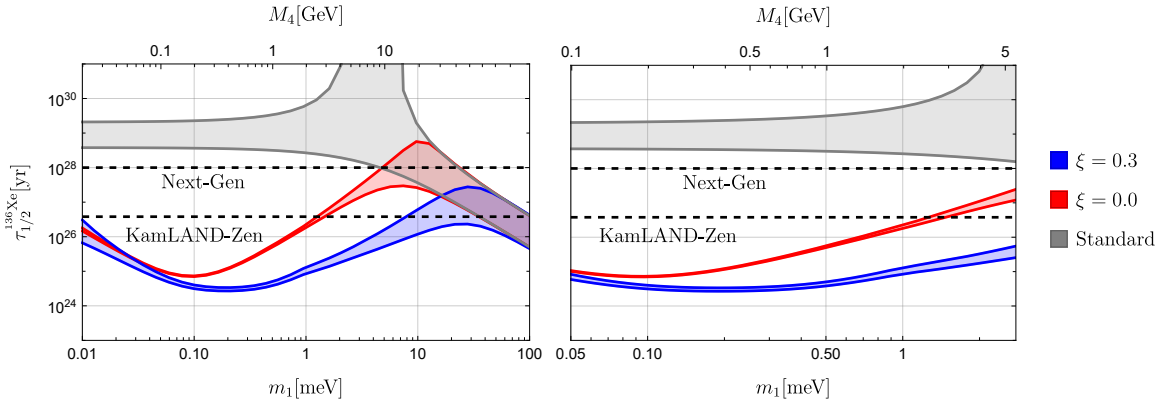

Figure 8. $0\nu\beta\beta$ lifetime of Xe^{136} in the type-II mLRSM in the NH as a function of the lightest (sterile) neutrino mass. We have set the heaviest sterile-neutrino mass at 100 GeV and $M_{W_R} = 10$ TeV and $\xi = 0.3$ (blue) and $\xi = 0$ (red). The gray regions correspond to the standard mechanism associated with the exchange of light active Majorana neutrinos without right-handed interactions. The right panel is the same as the left but zoomed in on the mass range most relevant for this work.

Because $\xi < 0.8$ [150] cannot be too large, the change in $\mathcal{A}^{\xi=0}$ in the first term is not too severe. The second term, however, can dominate $\mathcal{A}_R^{\xi}$. In particular, for $M_i \geq 1$ GeV, we can integrate out the sterile neutrinos, and the W_L-W_R mixing leads to dimension-nine lepton-number-violating operators of the form $(\bar{u}_L\gamma^\mu d_L)\,(\bar{u}_R\gamma^\mu d_R)\,\bar{e}_L C\bar{e}_L^T$. This operator has the right chiral properties to induce, at lower energies, processes of the form $\pi^-\pi^- \to e^-e^-$, which lead to enhanced $0\nu\beta\beta$ amplitudes once the pions are exchanged between nucleons in a nucleus [170, 172, 176]. This enhancement disappears for smaller $M_i \leq m_\pi$ but is still present for the sterile-neutrino masses we are interested in.

To illustrate the constraints that can be set from $0\nu\beta\beta$ experiments, we show the $0\nu\beta\beta$ lifetime of ^{136}Xe in figure 8 in the type-II limit in the NH as a function of the lightest neutrino mass m_1 (or equivalently, the lightest sterile neutrino mass M_4). We have set $M_6 = 100$ GeV and $M_{W_R} = 10$ TeV for concreteness and considered two cases for the W_L-W_R mixing parameters: $\xi = 0$ (red) and $\xi = 0.3$ (blue). The gray regions in both figures indicate the lifetime in the case of just three light Majorana neutrinos without contributions from sterile neutrinos or RH currents (we set $M_{W_R} \to \infty$). For $m_1 < 1$ meV, this leads to lifetimes of the order of 10^{29} y (the band is caused by marginalizing the unknown Majorana phases), roughly three orders of magnitude longer than the current best limit from KamLAND-Zen, $T_{1/2}^{0\nu} > 3.8 \cdot 10^{26}$ y [89], shown by the dashed horizontal line. We note that even the next-generation experiments, nEXO and LEGEND, projected to improve the sensitivities by a factor of ~ 100 [177, 178], cannot reach that, as shown also with a dashed horizontal line. In the mLRSM, the presence of relatively light sterile neutrinos that are charged under $SU(2)_R$, as indicated by the blue and red bands, can significantly reduce the lifetimes, reaching lifetimes around 10^{25} y for HNLs with masses of $\mathcal{O}(10^2)$ MeV. We obtain the width of the bands by marginalizing over the unknown Majorana phases and the phases α and θ_L. The effect of W_L-W_R mixing can be severe in this mass range because of the chiral enhancement discussed above. In the right panel of figure 8, we show the same results but now zoom in on the mass region for M_4 most relevant for displaced-vertex searches. We see that $0\nu\beta\beta$ limits rule out a large part of this parameter space even for a $M_{W_R} = 10$ TeV mass.

JHEP04(2025)007

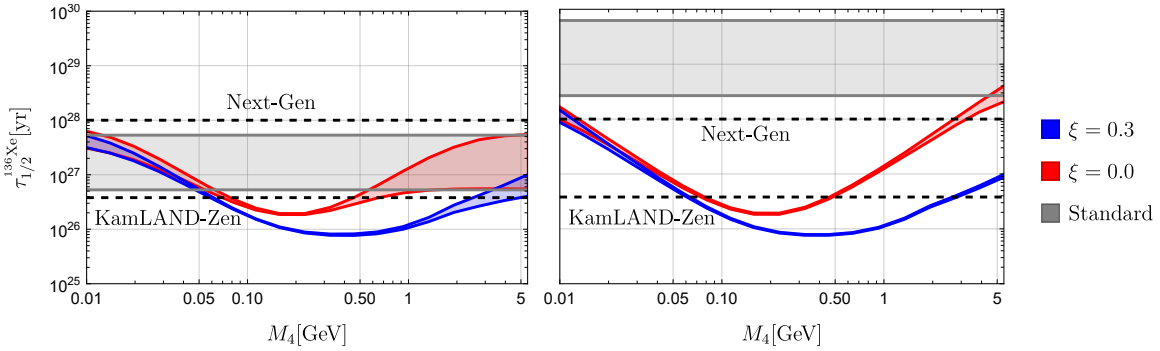

Figure 9. $0\nu\beta\beta$ lifetime of Xe^{136} in the type-I mLRSM in the NH as a function of the lightest HNL. We have set $m_1 = 0.03\,\text{eV}$ (left) and $m_1 = 0.001\,\text{eV}$ (right), $M_5 = M_6 = 100\,\text{GeV}$, $M_{W_R} = 15\,\text{TeV}$,and $\xi = 0.3$ (blue) and $\xi = 0$ (red). The gray regions correspond to the standard mechanism associated with the exchange of light active Majorana neutrinos without RH interactions.

We can perform very similar calculations in the type-I scenario. In this case, we need to specify the lightest neutrino mass, the hierarchy, and the values for all HNLs to compute the $0\nu\beta\beta$ lifetime. In figure 9, we have considered a scenario with $M_{W_R} = 15\,\text{TeV}$ for the lightest HNL in the mass region of interest, and we assumed the other HNLs to be significantly heavier. The difference between the left and right panel is the value of the lightest neutrino mass ($m_1 = 0.03\,\text{eV}$ left and $m_1 = 0.001\,\text{eV}$ right). As can be seen by comparing the two panels, the value of m_1 affects the $0\nu\beta\beta$ curves. Still, it barely influences the constraints on m_{W_R} because RH currents dominate the decay rates at the points where the current experimental limit is saturated.

7 Collider and fixed-target analysis

This section briefly introduces our computation method of estimating the expected number of observed sterile-neutrino-decay events in the considered experiments. We include the following `LHC` far-detector setups with the associated integrated luminosities: `ANUBIS` ($3\,\text{ab}^{-1}$) [122], `FASER` ($150\,\text{fb}^{-1}$) and `FASER2` ($3\,\text{ab}^{-1}$) [123, 124], `MATHUSLA` ($3\,\text{ab}^{-1}$) [33, 52, 125], `FACET` ($3\,\text{ab}^{-1}$) [126], `CODEX-b` ($300\,\text{fb}^{-1}$) [127], and `MoEDAL-MAPP1` ($30\,\text{fb}^{-1}$) and `MoEDAL-MAPP2` ($300\,\text{fb}^{-1}$) [128, 129]. For a more detailed summary of the `LHC` far-detector experiments, we refer to e.g. refs. [46, 48] and the references therein. We further investigate the `DUNE` (1.1×10^{22} protons on target (POTs)) near detector of the `LBNF` at Fermilab with a total run time of 10 years [113–117], and the recently approved `LHC` beam-dump experiment `SHiP` (2×10^{20} POTs) with five years' operation duration [49–51, 130]. We consider the case of a 120-GeV (400-GeV) proton beam hitting a target at `DUNE` (`SHiP`). The `DUNE` near detector [179, 180] employs a 194 m long decay pipe with a radius of 2 m placed 27 m downstream from the target, where the kaons are supposed to decay. Its near detector is constructed at a distance of 574 m downstream from the target and has a length of 6.4 m and a width of 3.5 m. The `SHiP` experiment [130] should instrument the detector with a distance of 45 m from the IP and a length of 50 m. With a pyramidal frustum shape, the detector has dimensions 1.5 m × 4.3 m (5 m × 10 m) with its front (rear) surface.

JHEP04(2025)007

Meson M	N_M (LHC)	N_M (DUNE)	N_M (SHiP)
$K^\pm$	2.38×10^{18}	5.76×10^{21}	1.9×10^{19}
K_L	1.31×10^{18}	5.76×10^{21}	1.9×10^{19}
K_S	1.31×10^{18}	5.76×10^{21}	1.9×10^{19}
$D^\pm$	2.04×10^{16}	2.28×10^{17}	1.4×10^{17}
D^0	3.89×10^{16}	6.95×10^{17}	4.3×10^{17}
$D_s^\pm$	6.62×10^{15}	9.68×10^{16}	6.0×10^{16}
$B^\pm$	1.46×10^{15}	4.46×10^{11}	2.7×10^{13}
B^0	1.46×10^{15}	4.46×10^{11}	2.7×10^{13}
B_s^0	2.53×10^{14}	1.11×10^{11}	7.2×10^{12}

Table 3. Number of mesons M over the full 4π solid angle [26, 40, 46, 48]. For the LHC, we show N_M for a center-of-mass energy of 14 TeV and a total integrated luminosity of $3\,\text{ab}^{-1}$. For DUNE with a proton beam energy of 120 GeV, N_M numbers are presented for a runtime of ten years with 1.1×10^{22} POTs. For SHiP with a proton beam energy of 400 GeV, we list N_M for a total operation time of 5 years with 2×10^{20} POTs. The superscript $\pm$ means the sum of the numbers of the positively charged and the negatively charged mesons. Similarly, D^0, B^0, and B_s^0 all denote the sum of the numbers of the two charge-conjugated states.

Next, we will discuss the computation of the number of produced sterile neutrinos. Considering sterile neutrinos originating from meson decays, N_{prod} is given by

$$N_{M,N}^{\text{prod}} = N_M \cdot \text{Br}(M \to N + X)\,, \tag{7.1}$$

where N_M is the number of mesons M produced at an experiment for its total runtime, which we list in table 3 for the LHC, DUNE, and SHiP experiments, and $\text{Br}(M \to N + X)$ is the branching ratio of a meson M into the final states that include a sterile neutrino (see section 4).

To evaluate the fraction of N_{prod} observed through sterile-neutrino decays in the detectors, we apply Monte-Carlo techniques to determine the geometrical acceptance for each detector setup. For a single N with speed β_i, boost factor γ_i and proper lifetime τ_N (see section 5) produced in the decay of a meson M, the probability of decaying inside the fiducial volume of a detector is given by

$$P_{M,i}[N \text{ in f.v.}] = \exp\left[-\frac{L_{T,i}}{\beta_i\gamma_i c\tau_N}\right]\left(1 - \exp\left[-\frac{L_{I,i}}{\beta_i\gamma_i c\tau_N}\right]\right). \tag{7.2}$$

Here, $L_{T,i}$ is the length N_i travels to reach the detector, $L_{I,i}$ is the length N_i would travel through the detector if it would not decay inside, and c is the speed of light. The values of $L_{T,i}$ and $L_{I,i}$ depend not only on the experiment on hand but also on the traveling direction of N_i as well as the vertex at which the meson decays into N_i. To understand their typical values, we

JHEP04(2025)007

refer to refs. [46, 48] for a summary of the geometrical setup of the experiments considered in this work. If N_i does not travel towards the detector, the decay probability inside the detector is zero. The charm and bottom mesons can be legitimately assumed to be decaying at the IP. However, we cannot do so for the kaons with their longer lifetimes. We thus also consider their displaced decay positions within the simulation. The computation should include only the kaons decaying before reaching areas of rock, shielding infrastructure, hadron absorbers, calorimeters, etc. For DUNE, there is no such problem as a specific decay pipe is instrumented at the near-detector experiment, while for the far detectors at the LHC, care should be taken and we refer to ref. [46] for the detail. For the SHiP experiment, the target is 1.4 m long [130], followed immediately by a hadron absorber and then muon shielding; thus, we require that the kaons decay before traveling one nuclear interaction length (~ 20 cm) into the target.

Using the event generator PYTHIA8 [181, 182] in combination with a three-dimensional approximation of the fiducial volume [46],[5] we simulate $N_{\rm MC} = 10^6$ proton-on-proton events with the corresponding beam-energy setups and calculate an average decay probability with

$$\langle P_M[N_i \text{ in f.v.}]\rangle = \frac{1}{N_{\rm MC}} \sum_i^{N_{\rm MC}} P_{M,i}[N \text{ in f.v.}]. \tag{7.3}$$

Lastly, the detector must be able to reconstruct the decay vertex of the sterile neutrino. We call final states 'visible' if we expect that the detector setup is capable of vertex reconstruction for that given final state. 'Invisible' final states, such as a final state consisting of only active neutrinos, are excluded from the analysis. The expected number of observed sterile-neutrino decays is given by

$$N_N^{\rm obs} = {\rm Br}(N \to \text{visible}) \sum_M N_{M,N}^{\rm prod} \cdot \langle P_M[N \text{ in f.v.}]\rangle \cdot h_M^{\rm decay}\,, \tag{7.4}$$

where ${\rm Br}(N \to \text{visible})$ is the branching ratio of the sterile neutrino into visible final states, and we assume 100% detection efficiency. $h_M^{\rm decay}$ is the fraction of the mesons M decaying in time, cf. the discussion below eq. (7.2). It is, therefore, equal to one for the charm and bottom mesons but is non-zero for kaons at the LHC far detectors and the SHiP experiment.

8 Numerical results

In the following, we discuss the results of the numerical simulations as introduced in the previous sections.

8.1 Type-II seesaw benchmark scenarios

We first analyze type-II seesaw scenarios with ($\xi = 0.3$) and without ($\xi = 0.0$) W_L-W_R mixing. In figure 10, we have drawn isocurves of $N_N^{\rm obs} = 3$ in the $M_4 - M_{W_R}$ plane for the LHC far detectors, DUNE near detector, and SHiP, as introduced in section 7. To simplify the presentation while obtaining the sensitivity reach to the RH gauge-boson mass, we assume a scenario where $M_{5,6} > m_{B_s}$, ensuring that only the lightest sterile neutrino N_4 is kinematically

[5] In the three-dimensional approximation we can include a meson traveling a macroscopic distance before decaying into the sterile neutrino. This allows us to include decays of the long-lived kaons in the analysis.

JHEP04(2025)007

relevant. We achieve this by selecting a sizable heaviest sterile-neutrino mass $M_6 = 100\,\text{GeV}$, cf. eq. (2.32). Choosing a substantially larger $M_6 = 1\,\text{TeV}$ would not significantly impact the results. Below the kaon threshold $M_4 < M_{K^\pm}$, DUNE has the highest sensitivity, whereas for $M_K^\pm < M_4 < M_D^\pm$ and $M_D^\pm < M_4 < M_{B_s}$, SHiP and MATHUSLA are predicted to have the strongest constraining power among the considered experiments, respectively. Furthermore, we display together the latest exclusion bounds of the $0\nu\beta\beta$ experiment KamLAND-Zen [89] on the RH gauge-boson mass. These limits were obtained by calculating the ^{136}Xe lifetime, as discussed in section 6. Here, to set the most conservative limits on M_{W_R}, we have maximized the ^{136}Xe lifetime over the unknown phases $\lambda_{1,2}$ and θ_L. Additionally, we depict the sensitivity reach of next-gen ton-scale experiments that are projected to probe the ^{136}Xe lifetime up to $\mathcal{O}(10^{28})$ years [177, 178]. We note that for M_4 below the pion threshold, the strongest sensitivity reach should, in principle, be derived by considering pion decays. We do not consider these decays in our simulation as our tool PYTHIA8 is not well validated for forward pion production. Therefore, we shade the corresponding parameter region with a light red color. Nevertheless, in this mass regime, the leading bounds on $|U_{e4}|^2$ were reported by the PIENU collaboration [183]. We have reinterpreted these bounds in terms of our model and will display them in the numerical results.

The left panel of figure 10 shows that the highest sensitivity reach to the RH gauge-boson masses for $0.1\,\text{GeV} < M_4 < 5\,\text{GeV}$ will be provided by next-generation $0\nu\beta\beta$ searches for $\xi = 0.3$. In this scenario, one can probe RH gauge-boson effects up to $M_{W_R} \sim 25\,\text{TeV}$ with these $0\nu\beta\beta$ experiments. Compared to the current $0\nu\beta\beta$ bounds on M_{W_R}, DUNE and SHiP are the only experiments that provide a competitive sensitivity reach, probing at most $M_{W_R} \sim 15\,\text{TeV}$. The right panel shows the same scenario but for $\xi = 0.0$. There, the DV searches can be competitive with next-generation $0\nu\beta\beta$ experiments. Below the kaon threshold, around $0.3\ \text{GeV} < M_4 < M_K^\pm$, DUNE and future $0\nu\beta\beta$ experiments exhibit similar sensitivity reach to RH currents. Above the kaon threshold, for $1.2\ \text{GeV} < M_4 < 1.9\ \text{GeV}$, SHiP outperforms the projected next-generation $0\nu\beta\beta$ experiments.

Below the kaon threshold, the most stringent upper limits on the minimal mixing angle $|U_{e4}|^2$ between the active and sterile neutrinos have been determined by the experiments NA62 [184] and T2K [185].[6] We translate these upper bounds into lower bounds on the RH gauge-boson mass, which agree with previous assessments [188]. We can compare these limits to the $0\nu\beta\beta$ constraints. For $\xi = 0.0$, current NA62 and T2K limits are competitive with current $0\nu\beta\beta$ constraints, whereas, for larger ξ, the $0\nu\beta\beta$ limits are more stringent. Upper bounds on the minimal mixing angle have also been determined by experiments such as CHARM [189, 190], DELPHI [191], PS191 [192, 193], BEBC [186, 187], and NuTeV [194]. Below the kaon threshold, these experiments' constraints are weaker than those of NA62 [184] and T2K [185], and we therefore do not show them. However, BEBC [186, 187] does extend the limits to larger sterile-neutrino masses leading the bounds on $|U_{e4}|^2$ for M_4 between the kaon and charm-meson thresholds, and its bounds are shown as dashed light-gray curves. They are much less stringent than the $0\nu\beta\beta$ limits.

[6] As mentioned above, in our numerical simulation we do not take into account the sterile neutrinos from pion decays which should dominate the sensitivity reach for $M_4 < m_\pi$, where the strongest present bounds on $|U_{e4}|^2$ were obtained at the PIENU experiment [183]. These bounds have been reinterpreted here in terms of our scenario.

JHEP04(2025)007

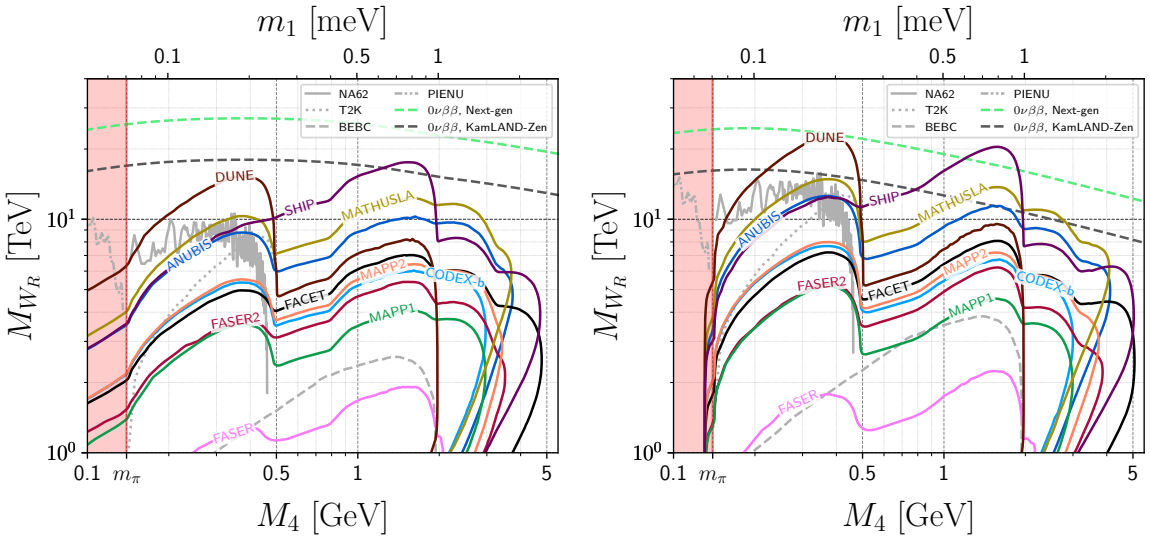

Figure 10. Predicted sensitivity reach of the next-gen $0\nu\beta\beta$ experiments and the DV searches (at the LHC far detectors, DUNE near detector, and beam-dump experiment SHiP) in the $M_4 - M_{W_R}$ plane in type-II seesaw scenarios. For the W_L-W_R mixing, we have set $\xi = 0.3$ ($\xi = 0$) in the left (right) panel. Also displayed are existing bounds obtained by recasting the results from the $0\nu\beta\beta$ experiment KamLAND-Zen [89] and the search for long-lived sterile neutrinos at the PIENU [183], NA62 [184], T2K [185], and BEBC [186, 187] experiments. The region for $M_4 < m_\pi$ is shaded in light red, as we do not include sterile neutrinos from pion decays in our simulation. We have set the heaviest sterile neutrino mass $M_6 = 100\,\text{GeV}$.

We predict that the sensitivity reach of (future) DV searches to M_{W_R} is stronger for $\xi = 0.0$ than for $\xi = 0.3$. Further, it is no coincidence that the DUNE sensitivity reach is most significantly impacted by non-zero values of ξ, as at DUNE predominantly (pseudoscalar) pions and kaons are produced, which are suppressed by the non-zero W_L-W_R mixing. Finally, as could be deduced from figure 8 (right), the $0\nu\beta\beta$ sensitivity reach is increased in a scenario with non-zero W_L-W_R mixing.

8.2 Type-I seesaw benchmark scenarios

Determining the sensitivity reaches of the considered experiments in type-I benchmark scenarios is only sensible when minimal-mixing contributions are significant compared to the RH-current contributions. Otherwise, these type-I seesaw scenarios converge to type-II seesaw scenarios, and we gain no new information. We again assume a scenario where only the lightest sterile neutrino N_4 is kinematically available. We determine whether the minimal-mixing or RH-current contributions dominate the sterile-neutrino production rate with eq. (4.4). For sterile-neutrino decays, we perform the same task numerically.

In figure 11, we show in the M_4-M_{W_R} plane whether the minimal-mixing contributions or RH-current contributions dominate the sterile-neutrino decay for various m_1 values. For example, we see that for a large $m_1 = 0.03\,\text{eV}$, the minimal-mixing contributions dominate the decays of the lightest sterile neutrinos for $M_4 < 0.9\,\text{GeV}$ (around the ρ-meson threshold) if $M_{W_R} \gtrsim 20\,\text{TeV}$. As shown in figure 10, DV-search experiments such as DUNE, SHiP, and

JHEP04(2025)007

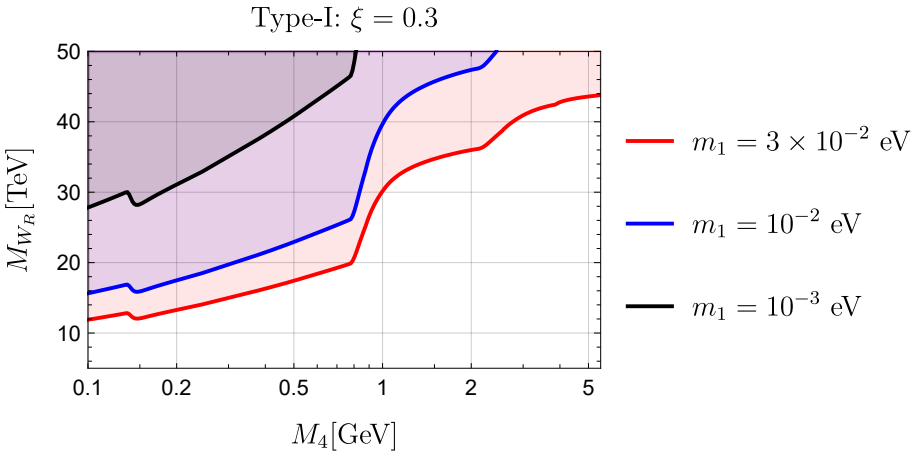

Figure 11. Isocurves in the M_4-M_{W_R} plane, corresponding to equal contributions from RH-current and minimal-mixing effects to sterile-neutrino decays for several m_1 values in type-I seesaw scenarios. Below (above) each of the isocurves, the RH-current (minimal-mixing) effects dominate.

MATHUSLA can probe RH gauge-boson effects in this mass range in type-II seesaw scenarios. This means minimal-mixing contributions can be significant for a relatively large m_1. Hence, we deem it interesting to analyze further the sensitivity reach in type-I seesaw benchmark scenarios, which we now do.

To maximize the impact of minimal-mixing effects, we set $m_1 = 0.03\,\text{eV}$. In figure 12, we show isocurves where $N_N^{\text{obs}} = 3$ for the (future) DV-search experiments in the considered type-I seesaw scenario. All the LHC far detectors that probe $\sim 10\,\text{TeV}$ RH gauge-boson masses exhibit similar isocurves compared to the type-II scenario. This is unsurprising as RH contributions dominate at this magnitude of M_{W_R}. However, in the case of DUNE, the sensitivity in the type-I seesaw scenario is perceptibly higher than in the type-II seesaw scenario. Finally, we note that the results are insensitive to the choice between generalized $\mathcal{P}$-symmetry and $\mathcal{C}$-symmetry scenarios.

Since there are no direct relations between the active- and sterile-neutrino masses in the type-I seesaw scenario, there is less predictive power for the $0\nu\beta\beta$ sensitivity reach compared to type-II seesaw scenarios. Nevertheless, comparing the $0\nu\beta\beta$ sensitivity reach to the far-detector sensitivity reaches is still interesting. We choose the sterile-neutrino masses to be large ($M_{5,6} = 100\,\text{GeV} \gg M_{B_s}$) to be conservative. In figure 12, we show the results for current and next-gen experiments in this type-I seesaw scenario. Again, the existing $0\nu\beta\beta$ constraints are stringent, but DUNE and SHiP will be more sensitive in parts of the parameter space.

Because of the relatively large m_1 at 0.03 eV, the minimal-mixing contributions are sufficiently large to be detected in next-generation $0\nu\beta\beta$ experiments for $M_4 > 0.5\,\text{GeV}$. This is true irrespective of the mass of the RH gauge boson, and therefore, the green dashed line becomes vertical. However, For $M_4 < 0.5\,\text{GeV}$, the active-neutrino contributions to the ^{136}Xe decay rate can cancel the sterile-neutrino contributions, analogous to the phase cancellations occurring in parts of the gray regions in figure 8. In this case, the next-generation $0\nu\beta\beta$ experiments will be sensitive to $M_{W_R} = 25\,\text{TeV}$ roughly.

JHEP04(2025)007

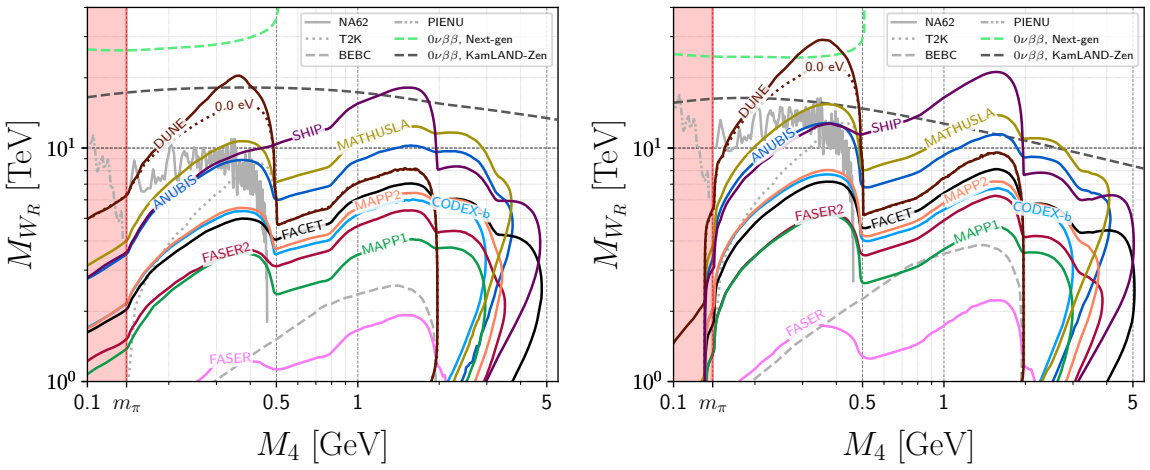

Figure 12. Predicted sensitivity reach of the next-gen $0\nu\beta\beta$ experiments and the DV searches in the $M_4 - M_{W_R}$ plane in the type-I seesaw scenario setting $m_1 = 0.03\,\text{eV}$. For the W_L-W_R mixing, we have set $\xi = 0.3$ ($\xi = 0.0$) in the left (right) panel. We also show existing bounds from the $0\nu\beta\beta$ experiment KamLAND-Zen [88]. We show recast bounds obtained from `PIENU` [183], `NA62` [184], `T2K` [185], and `BEBC` [186, 187].

9 Conclusions

Sterile neutrinos are prime candidates for explaining the lightness of the non-zero active neutrino masses via the seesaw mechanism. These elusive particles could also address other major issues in particle physics and cosmology, such as the baryon asymmetry of the Universe and dark matter. Relatively light, GeV-scale sterile neutrinos are particularly interesting because they can be copiously produced at numerous current and future particle-physics experiments. This work investigates the phenomenology of GeV-scale sterile neutrinos within the mLRSM. There, sterile neutrinos couple to SM particles through minimal mixing with active neutrinos and via heavy right-handed gauge bosons induced by a $\text{SU}(2)_R$ gauge symmetry at high energies. We have considered both type-II and type-I seesaw scenarios. For simplicity, we have assumed in most scenarios that only the lightest sterile-neutrino mass eigenstate N_4 is kinematically available.

For sterile-neutrino production and decay in DV searches, the essential benchmark parameters are the mass of the right-handed gauge boson M_{W_R} and the ratio of vevs $\xi = \kappa'/\kappa$, which sets the W_L-W_R mixing strength. In scenarios with a relatively large $\xi = 0.3$, hadronic processes may be significantly enhanced or suppressed through interference terms linear in ξ, depending on the parity configuration of initial and final-state particles.

In type-I seesaw scenarios, the left- and right-handed neutrino-mixing matrices U_{PMNS} and U_R are, in principle, uncorrelated. To reduce the number of free parameters, we assumed these two matrices were equal, as in type-II seesaw scenarios. In this limit, we note that for relatively light ($\lesssim 12\,\text{TeV}$) RH gauge-boson masses, minimal-mixing contributions induced by the non-zero Dirac mass term M_D are always sub-leading compared to RH-current contributions so that the type-I and type-II scenarios have a very similar phenomenology.

By performing Monte-Carlo simulations, we have investigated the sensitivity reaches of the following (future) DV experiments: `ANUBIS`, `CODEX-b`, `DUNE`, `FACET`, `FASER(2)`, `MATHUSLA`,

JHEP04(2025)007

MoEDAL-MAPP1(2), and SHiP. We have considered B-meson, D-meson, and kaon decays, where we have probed scenarios with and without the W_L-W_R mixing. We highlight the sensitivity reach of the DUNE and SHiP experiments, which could probe sterile-neutrino signal events for RH gauge-boson masses $\sim 20\,\text{TeV}$.

The presence of relatively light Majorana neutrinos with non-standard interactions with SM fields can lead to large neutrinoless double beta decay rates. We have computed these rates using modern EFT methods. In both type-I and type-II scenarios, there are several distinct contributions to the $0\nu\beta\beta$ rates. In particular, an exciting interplay exists in the type-I scenario between contributions from light active neutrinos and the HNLs with RH interactions. In scenarios with small W_L-W_R mixing, we find that the future DV searches at DUNE and SHiP will probe parameters space beyond the existing $0\nu\beta\beta$ bounds, including the future ton-scale program. Non-zero W_L-W_R mixing tends to increase $0\nu\beta\beta$ rates while suppressing the DV-search sensitivity, making $0\nu\beta\beta$ searches more competitive.

The large separation of scales between the masses of the light sterile neutrinos and the heavy RH gauge bosons present in the mLRSM allows the description of the physics studied here from another perspective, the EFT approach. The relevant EFT Lagrangians are νSMEFT and νLEFT, working above and below the EW scale, respectively. We have performed the matching between the mLRSM and the EFT Lagrangians. Previous studies applying EFT techniques for long-lived sterile neutrinos assume only specific Wilson coefficients with certain lepton- or quark-flavor configurations to be non-vanishing. While efficient, this approach considers scenarios that can be over-simplified from the view of UV completions. We have chosen to focus on the well-motivated UV-complete mLRSM analysis, which provides a more comprehensive phenomenology and, as shown, probes BSM scales comparable to those predicted with the EFT approach. However, an essential distinction between the two approaches is that a UV-complete model offers better predictability and allows for consistent consideration of complementary probes from sterile-neutrino-induced low-energy phenomena such as $0\nu\beta\beta$.

The main conclusion of this work is that in the mLRSM, the LHC far detectors, the DUNE near detector, and the beam-dump experiment SHiP at CERN can probe energy scales of the RH-current physics comparable to those that current and future $0\nu\beta\beta$ searches are sensitive to. Both DV and $0\nu\beta\beta$ searches are, therefore, essential for scrutinizing the existence of long-lived GeV-scale sterile neutrinos. Possible follow-up ideas of this work include investigating the correlation with constraints that can be set from Big Bang Nucleosynthesis. Additionally, it could be interesting to include sub-leading partonic processes in the DV searches and study their corresponding sensitivity results; in particular, they could have a more extensive mass reach on the sterile neutrino than the meson-decay events considered here.

Acknowledgments

Financial support for H.K.D. by the DFG (CRC 110, "Symmetries and the Emergence of Structure in QCD") is gratefully acknowledged. JdV and JeG acknowledge support from the Dutch Research Council(NWO) in the form of a VIDI grant.

JHEP04(2025)007

Data Availability Statement. This article has no associated data or the data will not be deposited.

Code Availability Statement. This article has no associated code or the code will not be deposited.

Open Access. This article is distributed under the terms of the Creative Commons Attribution License (CC-BY4.0), which permits any use, distribution and reproduction in any medium, provided the original author(s) and source are credited.

References

[1] Super-Kamiokande collaboration, *Evidence for oscillation of atmospheric neutrinos*, *Phys. Rev. Lett.* **81** (1998) 1562 [hep-ex/9807003] [INSPIRE].

[2] SNO collaboration, *Direct evidence for neutrino flavor transformation from neutral current interactions in the Sudbury Neutrino Observatory*, *Phys. Rev. Lett.* **89** (2002) 011301 [nucl-ex/0204008] [INSPIRE].

[3] Double Chooz collaboration, *Indication of Reactor $\bar{\nu}_e$ Disappearance in the Double Chooz Experiment*, *Phys. Rev. Lett.* **108** (2012) 131801 [arXiv:1112.6353] [INSPIRE].

[4] Daya Bay collaboration, *Observation of electron-antineutrino disappearance at Daya Bay*, *Phys. Rev. Lett.* **108** (2012) 171803 [arXiv:1203.1669] [INSPIRE].

[5] RENO collaboration, *Observation of Reactor Electron Antineutrino Disappearance in the RENO Experiment*, *Phys. Rev. Lett.* **108** (2012) 191802 [arXiv:1204.0626] [INSPIRE].

[6] T2K collaboration, *Observation of Electron Neutrino Appearance in a Muon Neutrino Beam*, *Phys. Rev. Lett.* **112** (2014) 061802 [arXiv:1311.4750] [INSPIRE].

[7] P. Minkowski, *$\mu \to e\gamma$ at a Rate of One Out of 10^9 Muon Decays?*, *Phys. Lett. B* **67** (1977) 421 [INSPIRE].

[8] T. Yanagida, *Horizontal gauge symmetry and masses of neutrinos*, *Conf. Proc. C* **7902131** (1979) 95 [INSPIRE].

[9] M. Gell-Mann, P. Ramond and R. Slansky, *Complex Spinors and Unified Theories*, *Conf. Proc. C* **790927** (1979) 315 [arXiv:1306.4669] [INSPIRE].

[10] R.N. Mohapatra and G. Senjanovic, *Neutrino Mass and Spontaneous Parity Nonconservation*, *Phys. Rev. Lett.* **44** (1980) 912 [INSPIRE].

[11] J. Schechter and J.W.F. Valle, *Neutrino Masses in SU(2) × U(1) Theories*, *Phys. Rev. D* **22** (1980) 2227 [INSPIRE].

[12] D. Wyler and L. Wolfenstein, *Massless Neutrinos in Left-Right Symmetric Models*, *Nucl. Phys. B* **218** (1983) 205 [INSPIRE].

[13] R.N. Mohapatra and J.W.F. Valle, *Neutrino Mass and Baryon Number Nonconservation in Superstring Models*, *Phys. Rev. D* **34** (1986) 1642 [INSPIRE].

[14] J. Bernabeu et al., *Lepton Flavor Nonconservation at High-Energies in a Superstring Inspired Standard Model*, *Phys. Lett. B* **187** (1987) 303 [INSPIRE].

[15] E.K. Akhmedov, M. Lindner, E. Schnapka and J.W.F. Valle, *Left-right symmetry breaking in NJL approach*, *Phys. Lett. B* **368** (1996) 270 [hep-ph/9507275] [INSPIRE].

JHEP04(2025)007

[16] E.K. Akhmedov, M. Lindner, E. Schnapka and J.W.F. Valle, *Dynamical left-right symmetry breaking*, *Phys. Rev. D* **53** (1996) 2752 [hep-ph/9509255] [INSPIRE].

[17] M. Malinsky, J.C. Romao and J.W.F. Valle, *Novel supersymmetric SO(10) seesaw mechanism*, *Phys. Rev. Lett.* **95** (2005) 161801 [hep-ph/0506296] [INSPIRE].

[18] F. Capozzi et al., *Unfinished fabric of the three neutrino paradigm*, *Phys. Rev. D* **104** (2021) 083031 [arXiv:2107.00532] [INSPIRE].

[19] I. Esteban et al., *The fate of hints: updated global analysis of three-flavor neutrino oscillations*, *JHEP* **09** (2020) 178 [arXiv:2007.14792] [INSPIRE].

[20] P.F. de Salas et al., *2020 global reassessment of the neutrino oscillation picture*, *JHEP* **02** (2021) 071 [arXiv:2006.11237] [INSPIRE].

[21] R.E. Shrock, *New Tests For, and Bounds On, Neutrino Masses and Lepton Mixing*, *Phys. Lett. B* **96** (1980) 159 [INSPIRE].

[22] R.E. Shrock, *General Theory of Weak Leptonic and Semileptonic Decays. 1. Leptonic Pseudoscalar Meson Decays, with Associated Tests For, and Bounds on, Neutrino Masses and Lepton Mixing*, *Phys. Rev. D* **24** (1981) 1232 [INSPIRE].

[23] R.E. Shrock, *General Theory of Weak Processes Involving Neutrinos. 2. Pure Leptonic Decays*, *Phys. Rev. D* **24** (1981) 1275 [INSPIRE].

[24] A.M. Abdullahi et al., *The present and future status of heavy neutral leptons*, *J. Phys. G* **50** (2023) 020501 [arXiv:2203.08039] [INSPIRE].

[25] A. Atre, T. Han, S. Pascoli and B. Zhang, *The Search for Heavy Majorana Neutrinos*, *JHEP* **05** (2009) 030 [arXiv:0901.3589] [INSPIRE].

[26] K. Bondarenko, A. Boyarsky, D. Gorbunov and O. Ruchayskiy, *Phenomenology of GeV-scale Heavy Neutral Leptons*, *JHEP* **11** (2018) 032 [arXiv:1805.08567] [INSPIRE].

[27] J.C. Helo, M. Hirsch and S. Kovalenko, *Heavy neutrino searches at the LHC with displaced vertices*, *Phys. Rev. D* **89** (2014) 073005 [*Erratum ibid.* **93** (2016) 099902] [arXiv:1312.2900] [INSPIRE].

[28] M. Drewes and J. Hajer, *Heavy Neutrinos in displaced vertex searches at the LHC and HL-LHC*, *JHEP* **02** (2020) 070 [arXiv:1903.06100] [INSPIRE].

[29] G. Cottin et al., *Long-lived heavy neutral leptons with a displaced shower signature at CMS*, *JHEP* **02** (2023) 011 [arXiv:2210.17446] [INSPIRE].

[30] W. Liu, J. Li, Z. Chen and H. Sun, *Probing Heavy Neutrinos at the LHC from Fat-jet using Machine Learning*, arXiv:2303.15920 [INSPIRE].

[31] J. Alimena et al., *Searching for long-lived particles beyond the Standard Model at the Large Hadron Collider*, *J. Phys. G* **47** (2020) 090501 [arXiv:1903.04497] [INSPIRE].

[32] L. Lee, C. Ohm, A. Soffer and T.-T. Yu, *Collider Searches for Long-Lived Particles Beyond the Standard Model*, *Prog. Part. Nucl. Phys.* **106** (2019) 210 [*Erratum ibid.* **122** (2022) 103912] [arXiv:1810.12602] [INSPIRE].

[33] D. Curtin et al., *Long-Lived Particles at the Energy Frontier: The MATHUSLA Physics Case*, *Rept. Prog. Phys.* **82** (2019) 116201 [arXiv:1806.07396] [INSPIRE].

[34] J. Beacham et al., *Physics Beyond Colliders at CERN: Beyond the Standard Model Working Group Report*, *J. Phys. G* **47** (2020) 010501 [arXiv:1901.09966] [INSPIRE].

JHEP04(2025)007

[35] F.F. Deppisch, P.S. Bhupal Dev and A. Pilaftsis, *Neutrinos and Collider Physics*, *New J. Phys.* **17** (2015) 075019 [arXiv:1502.06541] [INSPIRE].

[36] D.A. Bryman and R. Shrock, *Constraints on Sterile Neutrinos in the MeV to GeV Mass Range*, *Phys. Rev. D* **100** (2019) 073011 [arXiv:1909.11198] [INSPIRE].

[37] J.C. Helo, M. Hirsch and Z.S. Wang, *Heavy neutral fermions at the high-luminosity LHC*, *JHEP* **07** (2018) 056 [arXiv:1803.02212] [INSPIRE].

[38] G. Aielli et al., *Expression of interest for the CODEX-b detector*, *Eur. Phys. J. C* **80** (2020) 1177 [arXiv:1911.00481] [INSPIRE].

[39] B. Batell, J.A. Evans, S. Gori and M. Rai, *Dark Scalars and Heavy Neutral Leptons at DarkQuest*, *JHEP* **05** (2021) 049 [arXiv:2008.08108] [INSPIRE].

[40] I. Krasnov, *DUNE prospects in the search for sterile neutrinos*, *Phys. Rev. D* **100** (2019) 075023 [arXiv:1902.06099] [INSPIRE].

[41] P. Ballett, T. Boschi and S. Pascoli, *Heavy Neutral Leptons from low-scale seesaws at the DUNE Near Detector*, *JHEP* **03** (2020) 111 [arXiv:1905.00284] [INSPIRE].

[42] J.M. Berryman et al., *Searches for Decays of New Particles in the DUNE Multi-Purpose Near Detector*, *JHEP* **02** (2020) 174 [arXiv:1912.07622] [INSPIRE].

[43] P. Coloma et al., *GeV-scale neutrinos: interactions with mesons and DUNE sensitivity*, *Eur. Phys. J. C* **81** (2021) 78 [arXiv:2007.03701] [INSPIRE].

[44] DUNE collaboration, *Sensitivity to Heavy Neutral Leptons with the SAND detector at the DUNE ND complex*, arXiv:2209.01899 [INSPIRE].

[45] K.-J. Plows and X. Lu, *Modeling heavy neutral leptons in accelerator beamlines*, *Phys. Rev. D* **107** (2023) 055003 [arXiv:2211.10210] [INSPIRE].

[46] J.Y. Günther et al., *Long-lived neutral fermions at the DUNE near detector*, *JHEP* **01** (2024) 108 [arXiv:2310.12392] [INSPIRE].

[47] M. Hirsch and Z.S. Wang, *Heavy neutral leptons at ANUBIS*, *Phys. Rev. D* **101** (2020) 055034 [arXiv:2001.04750] [INSPIRE].

[48] J. De Vries et al., *Long-lived Sterile Neutrinos at the LHC in Effective Field Theory*, *JHEP* **03** (2021) 148 [arXiv:2010.07305] [INSPIRE].

[49] SHiP collaboration, *A facility to Search for Hidden Particles (SHiP) at the CERN SPS*, arXiv:1504.04956 [INSPIRE].

[50] S. Alekhin et al., *A facility to Search for Hidden Particles at the CERN SPS: the SHiP physics case*, *Rept. Prog. Phys.* **79** (2016) 124201 [arXiv:1504.04855] [INSPIRE].

[51] SHiP collaboration, *Sensitivity of the SHiP experiment to Heavy Neutral Leptons*, *JHEP* **04** (2019) 077 [arXiv:1811.00930] [INSPIRE].

[52] MATHUSLA collaboration, *An Update to the Letter of Intent for MATHUSLA: Search for Long-Lived Particles at the HL-LHC*, arXiv:2009.01693 [INSPIRE].

[53] F. Deppisch, S. Kulkarni and W. Liu, *Heavy neutrino production via Z' at the lifetime frontier*, *Phys. Rev. D* **100** (2019) 035005 [arXiv:1905.11889] [INSPIRE].

[54] C.-W. Chiang, G. Cottin, A. Das and S. Mandal, *Displaced heavy neutrinos from Z' decays at the LHC*, *JHEP* **12** (2019) 070 [arXiv:1908.09838] [INSPIRE].

[55] G. Cottin et al., *Displaced neutrino jets at the LHeC*, *JHEP* **06** (2022) 168 [arXiv:2104.13578] [INSPIRE].

JHEP04(2025)007

[56] A. Bhaskar et al., *Right-handed neutrino pair production via second-generation leptoquarks*, *Phys. Lett. B* **843** (2023) 138039 [arXiv:2301.11889] [INSPIRE].

[57] F. del Aguila, S. Bar-Shalom, A. Soni and J. Wudka, *Heavy Majorana Neutrinos in the Effective Lagrangian Description: Application to Hadron Colliders*, *Phys. Lett. B* **670** (2009) 399 [arXiv:0806.0876] [INSPIRE].

[58] A. Aparici, K. Kim, A. Santamaria and J. Wudka, *Right-handed neutrino magnetic moments*, *Phys. Rev. D* **80** (2009) 013010 [arXiv:0904.3244] [INSPIRE].

[59] S. Bhattacharya and J. Wudka, *Dimension-seven operators in the standard model with right handed neutrinos*, *Phys. Rev. D* **94** (2016) 055022 [*Erratum ibid.* **95** (2017) 039904] [arXiv:1505.05264] [INSPIRE].

[60] Y. Liao and X.-D. Ma, *Operators up to Dimension Seven in Standard Model Effective Field Theory Extended with Sterile Neutrinos*, *Phys. Rev. D* **96** (2017) 015012 [arXiv:1612.04527] [INSPIRE].

[61] G. Cottin et al., *Heavy neutral leptons in effective field theory and the high-luminosity LHC*, *JHEP* **09** (2021) 039 [arXiv:2105.13851] [INSPIRE].

[62] R. Beltrán et al., *Long-lived heavy neutral leptons at the LHC: four-fermion single-N_R operators*, *JHEP* **01** (2022) 044 [arXiv:2110.15096] [INSPIRE].

[63] G. Zhou et al., *Long-lived sterile neutrinos at Belle II in effective field theory*, *JHEP* **04** (2022) 057 [arXiv:2111.04403] [INSPIRE].

[64] R. Beltrán et al., *Long-lived heavy neutral leptons from mesons in effective field theory*, *JHEP* **01** (2023) 015 [arXiv:2210.02461] [INSPIRE].

[65] R. Beltrán et al., *Reinterpretation of searches for long-lived particles from meson decays*, *JHEP* **05** (2023) 031 [arXiv:2302.03216] [INSPIRE].

[66] R. Beltrán et al., *Heavy neutral leptons from kaons in effective field theory*, *Phys. Rev. D* **109** (2024) 115014 [arXiv:2309.11546] [INSPIRE].

[67] L. Duarte, G.A. González-Sprinberg and O.A. Sampayo, *Majorana neutrinos production at LHeC in an effective approach*, *Phys. Rev. D* **91** (2015) 053007 [arXiv:1412.1433] [INSPIRE].

[68] L. Duarte, J. Peressutti and O.A. Sampayo, *Not-that-heavy Majorana neutrino signals at the LHC*, *J. Phys. G* **45** (2018) 025001 [arXiv:1610.03894] [INSPIRE].

[69] T. Han, J. Liao, H. Liu and D. Marfatia, *Scalar and tensor neutrino interactions*, *JHEP* **07** (2020) 207 [arXiv:2004.13869] [INSPIRE].

[70] D. Barducci, E. Bertuzzo, A. Caputo and P. Hernandez, *Minimal flavor violation in the see-saw portal*, *JHEP* **06** (2020) 185 [arXiv:2003.08391] [INSPIRE].

[71] D. Barducci et al., *The see-saw portal at future Higgs Factories*, *JHEP* **03** (2021) 117 [arXiv:2011.04725] [INSPIRE].

[72] I. Bischer and W. Rodejohann, *General neutrino interactions from an effective field theory perspective*, *Nucl. Phys. B* **947** (2019) 114746 [arXiv:1905.08699] [INSPIRE].

[73] T. Li, X.-D. Ma and M.A. Schmidt, *General neutrino interactions with sterile neutrinos in light of coherent neutrino-nucleus scattering and meson invisible decays*, *JHEP* **07** (2020) 152 [arXiv:2005.01543] [INSPIRE].

[74] T. Li, X.-D. Ma and M.A. Schmidt, *Constraints on the charged currents in general neutrino interactions with sterile neutrinos*, *JHEP* **10** (2020) 115 [arXiv:2007.15408] [INSPIRE].

JHEP04(2025)007

[75] P.D. Bolton, F.F. Deppisch and C. Hati, *Probing new physics with long-range neutrino interactions: an effective field theory approach*, *JHEP* **07** (2020) 013 [arXiv:2004.08328] [INSPIRE].

[76] W. Dekens et al., *Sterile neutrinos and neutrinoless double beta decay in effective field theory*, *JHEP* **06** (2020) 097 [arXiv:2002.07182] [INSPIRE].

[77] V. Cirigliano et al., *Leptonic anomalous magnetic moments in ν SMEFT*, *JHEP* **08** (2021) 103 [arXiv:2105.11462] [INSPIRE].

[78] M. Chala and A. Titov, *One-loop running of dimension-six Higgs-neutrino operators and implications of a large neutrino dipole moment*, *JHEP* **09** (2020) 188 [arXiv:2006.14596] [INSPIRE].

[79] A. Datta, J. Kumar, H. Liu and D. Marfatia, *Anomalous dimensions from gauge couplings in SMEFT with right-handed neutrinos*, *JHEP* **02** (2021) 015 [arXiv:2010.12109] [INSPIRE].

[80] A. Datta, J. Kumar, H. Liu and D. Marfatia, *Anomalous dimensions from Yukawa couplings in SMNEFT: four-fermion operators*, *JHEP* **05** (2021) 037 [arXiv:2103.04441] [INSPIRE].

[81] CUORE collaboration, *Improved Limit on Neutrinoless Double-Beta Decay in ^{130}Te with CUORE*, *Phys. Rev. Lett.* **124** (2020) 122501 [arXiv:1912.10966] [INSPIRE].

[82] MAJORANA collaboration, *A Search for Neutrinoless Double-Beta Decay in ^{76}Ge with 26 kg-yr of Exposure from the MAJORANA DEMONSTRATOR*, *Phys. Rev. C* **100** (2019) 025501 [arXiv:1902.02299] [INSPIRE].

[83] CANDLES and LOW TEMPERATURE GROUP collaborations, *Status of ^{48}Ca double beta decay search and its future prospect in CANDLES*, *J. Phys. Conf. Ser.* **1468** (2020) 012132 [INSPIRE].

[84] GERDA collaboration, *Probing Majorana neutrinos with double-β decay*, *Science* **365** (2019) 1445 [arXiv:1909.02726] [INSPIRE].

[85] CUPID collaboration, *Final result of CUPID-0 phase-I in the search for the ^{82}Se Neutrinoless Double-β Decay*, *Phys. Rev. Lett.* **123** (2019) 032501 [arXiv:1906.05001] [INSPIRE].

[86] V. Alenkov et al., *First Results from the AMoRE-Pilot neutrinoless double beta decay experiment*, *Eur. Phys. J. C* **79** (2019) 791 [arXiv:1903.09483] [INSPIRE].

[87] EXO-200 collaboration, *Search for Neutrinoless Double-β Decay with the Complete EXO-200 Dataset*, *Phys. Rev. Lett.* **123** (2019) 161802 [arXiv:1906.02723] [INSPIRE].

[88] KAMLAND-ZEN collaboration, *Search for the Majorana Nature of Neutrinos in the Inverted Mass Ordering Region with KamLAND-Zen*, *Phys. Rev. Lett.* **130** (2023) 051801 [arXiv:2203.02139] [INSPIRE].

[89] KAMLAND-ZEN collaboration, *Search for Majorana Neutrinos with the Complete KamLAND-Zen Dataset*, arXiv:2406.11438 [INSPIRE].

[90] J.C. Pati and A. Salam, *Lepton Number as the Fourth Color*, *Phys. Rev. D* **10** (1974) 275 [INSPIRE].

[91] R.N. Mohapatra and J.C. Pati, *A Natural Left-Right Symmetry*, *Phys. Rev. D* **11** (1975) 2558 [INSPIRE].

[92] G. Senjanovic and R.N. Mohapatra, *Exact Left-Right Symmetry and Spontaneous Violation of Parity*, *Phys. Rev. D* **12** (1975) 1502 [INSPIRE].

[93] R.N. Mohapatra and G. Senjanovic, *Neutrino Masses and Mixings in Gauge Models with Spontaneous Parity Violation*, *Phys. Rev. D* **23** (1981) 165 [INSPIRE].

JHEP04(2025)007

[94] G. Senjanovic, *Spontaneous Breakdown of Parity in a Class of Gauge Theories*, *Nucl. Phys. B* **153** (1979) 334 [INSPIRE].

[95] S.L. Glashow, *The Future of Elementary Particle Physics*, *NATO Sci. Ser. B* **61** (1980) 687 [INSPIRE].

[96] M. Nemevsek, G. Senjanovic and Y. Zhang, *Warm Dark Matter in Low Scale Left-Right Theory*, *JCAP* **07** (2012) 006 [arXiv:1205.0844] [INSPIRE].

[97] M. Nemevšek and Y. Zhang, *Anatomy of diluted dark matter in the minimal left-right symmetric model*, *Phys. Rev. D* **109** (2024) 056021 [arXiv:2312.00129] [INSPIRE].

[98] M. Fukugita and T. Yanagida, *Baryogenesis Without Grand Unification*, *Phys. Lett. B* **174** (1986) 45 [INSPIRE].

[99] J.-M. Frere, T. Hambye and G. Vertongen, *Is leptogenesis falsifiable at LHC?*, *JHEP* **01** (2009) 051 [arXiv:0806.0841] [INSPIRE].

[100] P.S. Bhupal Dev, C.-H. Lee and R.N. Mohapatra, *Leptogenesis Constraints on the Mass of Right-handed Gauge Bosons*, *Phys. Rev. D* **90** (2014) 095012 [arXiv:1408.2820] [INSPIRE].

[101] P.S. Bhupal Dev, C.-H. Lee and R.N. Mohapatra, *TeV Scale Lepton Number Violation and Baryogenesis*, *J. Phys. Conf. Ser.* **631** (2015) 012007 [arXiv:1503.04970] [INSPIRE].

[102] M. Dhuria, C. Hati, R. Rangarajan and U. Sarkar, *Falsifying leptogenesis for a TeV scale $W_R^\pm$ at the LHC*, *Phys. Rev. D* **92** (2015) 031701 [arXiv:1503.07198] [INSPIRE].

[103] P.S. Bhupal Dev, R.N. Mohapatra and Y. Zhang, *CP Violating Effects in Heavy Neutrino Oscillations: Implications for Colliders and Leptogenesis*, *JHEP* **11** (2019) 137 [arXiv:1904.04787] [INSPIRE].

[104] CMS collaboration, *Search for a right-handed W boson and a heavy neutrino in proton-proton collisions at $\sqrt{s} = 13$ TeV*, *JHEP* **04** (2022) 047 [arXiv:2112.03949] [INSPIRE].

[105] ATLAS collaboration, *Search for heavy Majorana or Dirac neutrinos and right-handed W gauge bosons in final states with charged leptons and jets in pp collisions at $\sqrt{s} = 13$ TeV with the ATLAS detector*, *Eur. Phys. J. C* **83** (2023) 1164 [arXiv:2304.09553] [INSPIRE].

[106] CMS collaboration, *Search for Z' bosons decaying to pairs of heavy Majorana neutrinos in proton-proton collisions at $\sqrt{s} = 13$ TeV*, *JHEP* **11** (2023) 181 [arXiv:2307.06959] [INSPIRE].

[107] O. Mikulenko, *Quasi-Dirac Heavy Neutral Leptons in the Left-Right Symmetric Model*, arXiv:2406.13850 [INSPIRE].

[108] R. Kuchimanchi, *Leptonic CP problem in left-right symmetric model*, *Phys. Rev. D* **91** (2015) 071901 [arXiv:1408.6382] [INSPIRE].

[109] G. Senjanovic and V. Tello, *Strong CP violation: Problem or blessing?*, *Int. J. Mod. Phys. A* **38** (2023) 2350067 [arXiv:2004.04036] [INSPIRE].

[110] G. Li, D.-Y. Luo and X. Zhao, *Calculable neutrino Dirac mass matrix and one-loop θ^- in the minimal left-right symmetric model*, *Phys. Rev. D* **110** (2024) 035030 [arXiv:2404.16740] [INSPIRE].

[111] G. Li, M.J. Ramsey-Musolf and J.C. Vasquez, *Unraveling the left-right mixing using $0\nu\beta\beta$ decay and collider probes*, *Phys. Rev. D* **105** (2022) 115021 [arXiv:2202.01789] [INSPIRE].

[112] K.A. Urquía-Calderón, *Long-lived heavy neutral leptons at lepton colliders as a probe of left-right-symmetric models*, *Phys. Rev. D* **109** (2024) 055002 [arXiv:2310.17406] [INSPIRE].

JHEP04(2025)007

[113] DUNE collaboration, *Deep Underground Neutrino Experiment (DUNE), Far Detector Technical Design Report, Volume I Introduction to DUNE*, 2020 *JINST* **15** T08008 [arXiv:2002.02967] [INSPIRE].

[114] DUNE collaboration, *Deep Underground Neutrino Experiment (DUNE), Far Detector Technical Design Report, Volume II: DUNE Physics*, arXiv:2002.03005 [INSPIRE].

[115] DUNE collaboration, *Long-baseline neutrino oscillation physics potential of the DUNE experiment*, *Eur. Phys. J. C* **80** (2020) 978 [arXiv:2006.16043] [INSPIRE].

[116] DUNE collaboration, *Experiment Simulation Configurations Approximating DUNE TDR*, arXiv:2103.04797 [INSPIRE].

[117] DUNE collaboration, *Low exposure long-baseline neutrino oscillation sensitivity of the DUNE experiment*, *Phys. Rev. D* **105** (2022) 072006 [arXiv:2109.01304] [INSPIRE].

[118] CMS collaboration, *Recording and reconstructing 10 billion unbiased b hadron decays in CMS*, *EPJ Web Conf.* **245** (2020) 01025 [INSPIRE].

[119] CMS collaboration, *Test of lepton flavor universality in $B^{\pm} \to K^{\pm}\mu^{+}\mu^{-}$ and $B^{\pm} \to K^{\pm}e^{+}e^{-}$ decays in proton-proton collisions at $\sqrt{s} = 13$ TeV*, *Rept. Prog. Phys.* **87** (2024) 077802 [arXiv:2401.07090] [INSPIRE].

[120] CMS collaboration, *Enriching the Physics Program of the CMS Experiment via Data Scouting and Data Parking*, arXiv:2403.16134 [INSPIRE].

[121] CMS collaboration, *Search for long-lived heavy neutrinos in the decays of B mesons produced in proton-proton collisions at $\sqrt{s} = 13$ TeV*, *JHEP* **06** (2024) 183 [arXiv:2403.04584] [INSPIRE].

[122] M. Bauer, O. Brandt, L. Lee and C. Ohm, *ANUBIS: Proposal to search for long-lived neutral particles in CERN service shafts*, arXiv:1909.13022 [INSPIRE].

[123] J.L. Feng, I. Galon, F. Kling and S. Trojanowski, *ForwArd Search ExpeRiment at the LHC*, *Phys. Rev. D* **97** (2018) 035001 [arXiv:1708.09389] [INSPIRE].

[124] FASER collaboration, *FASER's physics reach for long-lived particles*, *Phys. Rev. D* **99** (2019) 095011 [arXiv:1811.12522] [INSPIRE].

[125] J.P. Chou, D. Curtin and H.J. Lubatti, *New Detectors to Explore the Lifetime Frontier*, *Phys. Lett. B* **767** (2017) 29 [arXiv:1606.06298] [INSPIRE].

[126] S. Cerci et al., *FACET: A new long-lived particle detector in the very forward region of the CMS experiment*, *JHEP* **06** (2022) 110 [arXiv:2201.00019] [INSPIRE].

[127] V.V. Gligorov, S. Knapen, M. Papucci and D.J. Robinson, *Searching for Long-lived Particles: A Compact Detector for Exotics at LHCb*, *Phys. Rev. D* **97** (2018) 015023 [arXiv:1708.09395] [INSPIRE].

[128] J.L. Pinfold, *The MoEDAL Experiment at the LHC — A Progress Report*, *Universe* **5** (2019) 47 [INSPIRE].

[129] J.L. Pinfold, *The MoEDAL experiment: a new light on the high-energy frontier*, *Phil. Trans. Roy. Soc. Lond. A* **377** (2019) 20190382 [INSPIRE].

[130] SHiP collaboration, *The SHiP experiment at the proposed CERN SPS Beam Dump Facility*, *Eur. Phys. J. C* **82** (2022) 486 [arXiv:2112.01487] [INSPIRE].

[131] P. Bamert, C.P. Burgess and R.N. Mohapatra, *Heavy sterile neutrinos and neutrinoless double beta decay*, *Nucl. Phys. B* **438** (1995) 3 [hep-ph/9408367] [INSPIRE].

JHEP04(2025)007

[132] M. Blennow, E. Fernandez-Martinez, J. Lopez-Pavon and J. Menendez, *Neutrinoless double beta decay in seesaw models*, *JHEP* **07** (2010) 096 [arXiv:1005.3240] [INSPIRE].

[133] M. Mitra, G. Senjanovic and F. Vissani, *Neutrinoless Double Beta Decay and Heavy Sterile Neutrinos*, *Nucl. Phys. B* **856** (2012) 26 [arXiv:1108.0004] [INSPIRE].

[134] A. de Gouvea and W.-C. Huang, *Constraining the (Low-Energy) Type-I Seesaw*, *Phys. Rev. D* **85** (2012) 053006 [arXiv:1110.6122] [INSPIRE].

[135] Y.F. Li and S.-S. Liu, *Vanishing effective mass of the neutrinoless double beta decay including light sterile neutrinos*, *Phys. Lett. B* **706** (2012) 406 [arXiv:1110.5795] [INSPIRE].

[136] J. Barry and W. Rodejohann, *Lepton number and flavour violation in TeV-scale left-right symmetric theories with large left-right mixing*, *JHEP* **09** (2013) 153 [arXiv:1303.6324] [INSPIRE].

[137] M. Ghosh, S. Goswami, S. Gupta and C.S. Kim, *Implication of a vanishing element in the 3+1 scenario*, *Phys. Rev. D* **88** (2013) 033009 [arXiv:1305.0180] [INSPIRE].

[138] I. Girardi, A. Meroni and S.T. Petcov, *Neutrinoless Double Beta Decay in the Presence of Light Sterile Neutrinos*, *JHEP* **11** (2013) 146 [arXiv:1308.5802] [INSPIRE].

[139] J. Barea, J. Kotila and F. Iachello, *Limits on sterile neutrino contributions to neutrinoless double beta decay*, *Phys. Rev. D* **92** (2015) 093001 [arXiv:1509.01925] [INSPIRE].

[140] P.D. Bolton, F.F. Deppisch and P.S. Bhupal Dev, *Neutrinoless double beta decay versus other probes of heavy sterile neutrinos*, *JHEP* **03** (2020) 170 [arXiv:1912.03058] [INSPIRE].

[141] T. Asaka, H. Ishida and K. Tanaka, *Hiding neutrinoless double beta decay in the minimal seesaw mechanism*, *Phys. Rev. D* **103** (2021) 015014 [arXiv:2012.12564] [INSPIRE].

[142] T. Jha, S. Khan, M. Mitra and A. Patra, *Zooming in on eV-MeV scale sterile neutrinos in light of neutrinoless double beta decay*, *Phys. Rev. D* **105** (2022) 035001 [arXiv:2107.03807] [INSPIRE].

[143] W. Dekens et al., *Neutrinoless double beta decay rates in the presence of light sterile neutrinos*, *JHEP* **09** (2024) 201 [arXiv:2402.07993] [INSPIRE].

[144] N.G. Deshpande, J.F. Gunion, B. Kayser and F.I. Olness, *Left-right symmetric electroweak models with triplet Higgs*, *Phys. Rev. D* **44** (1991) 837 [INSPIRE].

[145] A. Melfo et al., *Type II Seesaw at LHC: The Roadmap*, *Phys. Rev. D* **85** (2012) 055018 [arXiv:1108.4416] [INSPIRE].

[146] E. Fernandez-Martinez, J. Hernandez-Garcia and J. Lopez-Pavon, *Global constraints on heavy neutrino mixing*, *JHEP* **08** (2016) 033 [arXiv:1605.08774] [INSPIRE].

[147] G. Senjanovic, *Neutrino mass: From LHC to grand unification*, *Riv. Nuovo Cim.* **34** (2011) 1 [INSPIRE].

[148] M. Nemevsek, G. Senjanovic and V. Tello, *Connecting Dirac and Majorana Neutrino Mass Matrices in the Minimal Left-Right Symmetric Model*, *Phys. Rev. Lett.* **110** (2013) 151802 [arXiv:1211.2837] [INSPIRE].

[149] G. Senjanović and V. Tello, *Probing Seesaw with Parity Restoration*, *Phys. Rev. Lett.* **119** (2017) 201803 [arXiv:1612.05503] [INSPIRE].

[150] A. Maiezza, M. Nemevsek, F. Nesti and G. Senjanovic, *Left-Right Symmetry at LHC*, *Phys. Rev. D* **82** (2010) 055022 [arXiv:1005.5160] [INSPIRE].

JHEP04(2025)007

[151] G. Senjanović and V. Tello, *Restoration of Parity and the Right-Handed Analog of the CKM Matrix*, *Phys. Rev. D* **94** (2016) 095023 [arXiv:1502.05704] [INSPIRE].

[152] G. Senjanović and V. Tello, *Right Handed Quark Mixing in Left-Right Symmetric Theory*, *Phys. Rev. Lett.* **114** (2015) 071801 [arXiv:1408.3835] [INSPIRE].

[153] PARTICLE DATA GROUP collaboration, *Review of Particle Physics*, *PTEP* **2022** (2022) 083C01 [INSPIRE].

[154] S. Bertolini, A. Maiezza and F. Nesti, *Kaon CP violation and neutron EDM in the minimal left-right symmetric model*, *Phys. Rev. D* **101** (2020) 035036 [arXiv:1911.09472] [INSPIRE].

[155] W. Dekens et al., *A low-energy perspective on the minimal left-right symmetric model*, *JHEP* **11** (2021) 127 [arXiv:2107.10852] [INSPIRE].

[156] J. de Vries, G. Li, M.J. Ramsey-Musolf and J.C. Vasquez, *Light sterile neutrinos, left-right symmetry, and $0\nu\beta\beta$ decay*, *JHEP* **11** (2022) 056 [arXiv:2209.03031] [INSPIRE].

[157] E. Giusarma et al., *Improvement of cosmological neutrino mass bounds*, *Phys. Rev. D* **94** (2016) 083522 [arXiv:1605.04320] [INSPIRE].

[158] S. Vagnozzi et al., *Unveiling ν secrets with cosmological data: neutrino masses and mass hierarchy*, *Phys. Rev. D* **96** (2017) 123503 [arXiv:1701.08172] [INSPIRE].

[159] S. Vagnozzi et al., *Constraints on the sum of the neutrino masses in dynamical dark energy models with $w(z) \geq -1$ are tighter than those obtained in ΛCDM*, *Phys. Rev. D* **98** (2018) 083501 [arXiv:1801.08553] [INSPIRE].

[160] I. Tanseri et al., *Updated neutrino mass constraints from galaxy clustering and CMB lensing-galaxy cross-correlation measurements*, *JHEAp* **36** (2022) 1 [arXiv:2207.01913] [INSPIRE].

[161] PLANCK collaboration, *Planck 2018 results. VI. Cosmological parameters*, *Astron. Astrophys.* **641** (2020) A6 [*Erratum ibid.* **652** (2021) C4] [arXiv:1807.06209] [INSPIRE].

[162] M.L. Perl, *The Tau lepton*, *Rept. Prog. Phys.* **55** (1992) 653 [INSPIRE].

[163] E. Braaten, S. Narison and A. Pich, *QCD analysis of the tau hadronic width*, *Nucl. Phys. B* **373** (1992) 581 [INSPIRE].

[164] S.G. Gorishnii, A.L. Kataev and S.A. Larin, *The $O(\alpha_s^3)$-corrections to $\sigma_{\rm tot}(e^+e^- \to hadrons)$ and $\Gamma(\tau^- \to \nu_\tau + hadrons)$ in QCD*, *Phys. Lett. B* **259** (1991) 144 [INSPIRE].

[165] M. Doi, T. Kotani and E. Takasugi, *Double beta Decay and Majorana Neutrino*, *Prog. Theor. Phys. Suppl.* **83** (1985) 1 [INSPIRE].

[166] W. Rodejohann, *Neutrino-less Double Beta Decay and Particle Physics*, *Int. J. Mod. Phys. E* **20** (2011) 1833 [arXiv:1106.1334] [INSPIRE].

[167] M. Nemevsek, F. Nesti, G. Senjanovic and V. Tello, *Neutrinoless Double Beta Decay: Low Left-Right Symmetry Scale?*, arXiv:1112.3061 [INSPIRE].

[168] P.S. Bhupal Dev, S. Goswami and M. Mitra, *TeV Scale Left-Right Symmetry and Large Mixing Effects in Neutrinoless Double Beta Decay*, *Phys. Rev. D* **91** (2015) 113004 [arXiv:1405.1399] [INSPIRE].

[169] G. Li, M. Ramsey-Musolf and J.C. Vasquez, *Left-Right Symmetry and Leading Contributions to Neutrinoless Double Beta Decay*, *Phys. Rev. Lett.* **126** (2021) 151801 [arXiv:2009.01257] [INSPIRE].

JHEP04(2025)007

[170] G. Prezeau, M. Ramsey-Musolf and P. Vogel, *Neutrinoless double beta decay and effective field theory*, *Phys. Rev. D* **68** (2003) 034016 [hep-ph/0303205] [INSPIRE].

[171] V. Cirigliano et al., *Neutrinoless double beta decay in chiral effective field theory: lepton number violation at dimension seven*, *JHEP* **12** (2017) 082 [arXiv:1708.09390] [INSPIRE].

[172] V. Cirigliano et al., *A neutrinoless double beta decay master formula from effective field theory*, *JHEP* **12** (2018) 097 [arXiv:1806.02780] [INSPIRE].

[173] L. Graf, F.F. Deppisch, F. Iachello and J. Kotila, *Short-Range Neutrinoless Double Beta Decay Mechanisms*, *Phys. Rev. D* **98** (2018) 095023 [arXiv:1806.06058] [INSPIRE].

[174] F.F. Deppisch, L. Graf, F. Iachello and J. Kotila, *Analysis of light neutrino exchange and short-range mechanisms in $0\nu\beta\beta$ decay*, *Phys. Rev. D* **102** (2020) 095016 [arXiv:2009.10119] [INSPIRE].

[175] W. Dekens et al., *Neutrinoless double-β decay in the neutrino-extended standard model*, *Phys. Rev. C* **108** (2023) 045501 [arXiv:2303.04168] [INSPIRE].

[176] A. Nicholson et al., *Heavy physics contributions to neutrinoless double beta decay from QCD*, *Phys. Rev. Lett.* **121** (2018) 172501 [arXiv:1805.02634] [INSPIRE].

[177] nEXO collaboration, *Sensitivity and Discovery Potential of nEXO to Neutrinoless Double Beta Decay*, *Phys. Rev. C* **97** (2018) 065503 [arXiv:1710.05075] [INSPIRE].

[178] LEGEND collaboration, *The Large Enriched Germanium Experiment for Neutrinoless Double Beta Decay (LEGEND)*, *AIP Conf. Proc.* **1894** (2017) 020027 [arXiv:1709.01980] [INSPIRE].

[179] DUNE collaboration, *Long-Baseline Neutrino Facility (LBNF) and Deep Underground Neutrino Experiment (DUNE): Conceptual Design Report, Volume 3: Long-Baseline Neutrino Facility for DUNE June 24, 2015*, arXiv:1601.05823 [INSPIRE].

[180] DUNE collaboration, *Long-Baseline Neutrino Facility (LBNF) and Deep Underground Neutrino Experiment (DUNE): Conceptual Design Report, Volume 4 The DUNE Detectors at LBNF*, arXiv:1601.02984 [INSPIRE].

[181] C. Bierlich et al., *A comprehensive guide to the physics and usage of PYTHIA 8.3*, *SciPost Phys. Codeb.* **2022** (2022) 8 [arXiv:2203.11601] [INSPIRE].

[182] T. Sjöstrand et al., *An introduction to PYTHIA 8.2*, *Comput. Phys. Commun.* **191** (2015) 159 [arXiv:1410.3012] [INSPIRE].

[183] PIENU collaboration, *Search for heavy neutrinos in $\pi \to \mu\nu$ decay*, *Phys. Lett. B* **798** (2019) 134980 [arXiv:1904.03269] [INSPIRE].

[184] NA62 collaboration, *Search for heavy neutral lepton production in K+ decays to positrons*, *Phys. Lett. B* **807** (2020) 135599 [arXiv:2005.09575] [INSPIRE].

[185] T2K collaboration, *Search for heavy neutrinos with the T2K near detector ND280*, *Phys. Rev. D* **100** (2019) 052006 [arXiv:1902.07598] [INSPIRE].

[186] WA66 collaboration, *Search for Heavy Neutrino Decays in the BEBC Beam Dump Experiment*, *Phys. Lett. B* **160** (1985) 207 [INSPIRE].

[187] R. Barouki, G. Marocco and S. Sarkar, *Blast from the past II: Constraints on heavy neutral leptons from the BEBC WA66 beam dump experiment*, *SciPost Phys.* **13** (2022) 118 [arXiv:2208.00416] [INSPIRE].

[188] G.F.S. Alves, C.S. Fong, L.P.S. Leal and R. Zukanovich Funchal, *Limits on WR from Meson Decays*, *Phys. Rev. Lett.* **133** (2024) 161802 [arXiv:2307.04862] [INSPIRE].

JHEP04(2025)007

[189] CHARM collaboration, *A Search for Decays of Heavy Neutrinos in the Mass Range 0.5-GeV to 2.8-GeV*, *Phys. Lett. B* **166** (1986) 473 [INSPIRE].

[190] J. Orloff, A.N. Rozanov and C. Santoni, *Limits on the mixing of tau neutrino to heavy neutrinos*, *Phys. Lett. B* **550** (2002) 8 [hep-ph/0208075] [INSPIRE].

[191] DELPHI collaboration, *Search for neutral heavy leptons produced in Z decays*, *Z. Phys. C* **74** (1997) 57 [*Erratum ibid.* **75** (1997) 580] [INSPIRE].

[192] G. Bernardi et al., *Further limits on heavy neutrino couplings*, *Phys. Lett. B* **203** (1988) 332 [INSPIRE].

[193] O. Ruchayskiy and A. Ivashko, *Experimental bounds on sterile neutrino mixing angles*, *JHEP* **06** (2012) 100 [arXiv:1112.3319] [INSPIRE].

[194] NuTeV and E815 collaborations, *Search for neutral heavy leptons in a high-energy neutrino beam*, *Phys. Rev. Lett.* **83** (1999) 4943 [hep-ex/9908011] [INSPIRE].

JHEP04(2025)007